AD-A034 586 DAVID W TAYLOR NAVAL SHIP RESEARCH AND DEVELOPMENT CE--ETC F/G 13/10
EFFECTS OF BOUNDARY-LAYER DEVELOPMENT ON CAVITATION NOISE AND I--ETC(U)
DEC 76 W K BLAKE, M J WOLPERT, F E GEIB

UNCLASSIFIED DTNSRDC-76-0051 NL

1 OF 1
AD
A034586

END

DATE
FILMED
2-77

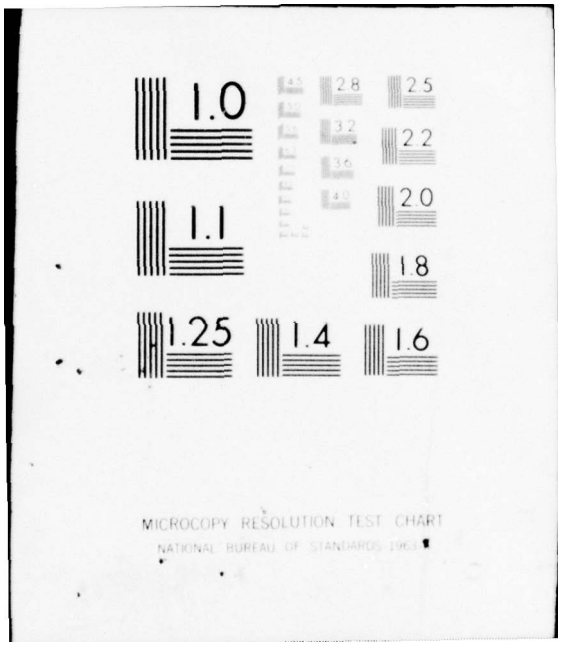
1.0
1.1
1.25
1.4
1.6
1.8
2.0
2.2
2.5
2.8
3.2
3.6
4.0
MICROCOPY RESOLUTION TEST CHART
NATIONAL BUREAU OF STANDARDS 1963

DAVID W. TAYLOR NAVAL SHIP RESEARCH AND DEVELOPMENT CENTER

Bethesda, Md. 20084

EFFECTS OF BOUNDARY-LAYER DEVELOPMENT ON CAVITATION NOISE AND INCEPTION ON A HYDROFOIL

by

William K. Blake, Melvin J. Wolpert, III,
Frank E. Geib, Jr., and Henry T. Wang

SHIP ACOUSTICS DEPARTMENT
RESEARCH AND DEVELOPMENT REPORT

December 1976 Report 76-0051

MAJOR DTNSRDC ORGANIZATIONAL COMPONENTS

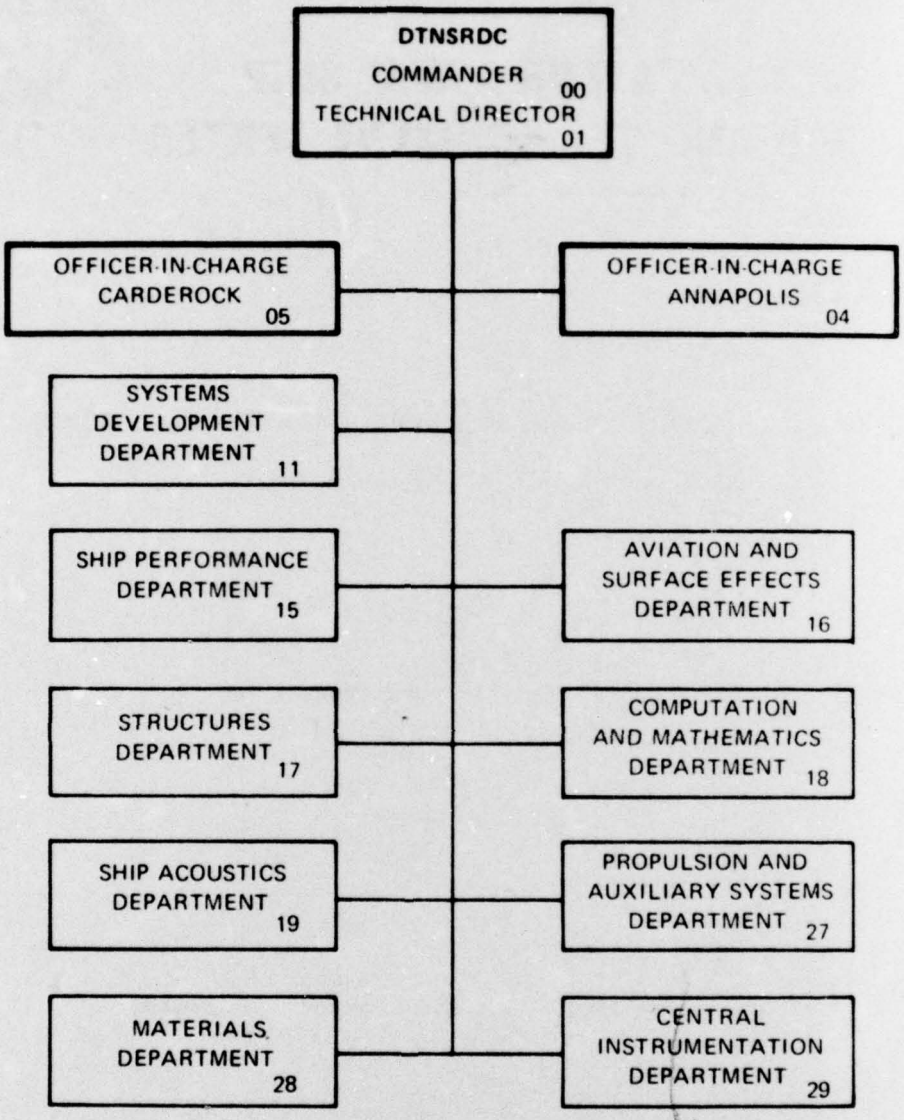

GPO 905-678

NDW-DTNSRDC 3960/43b (Rev. 11-75)
GPO 928-108

DTNSRDC ISSUES THREE TYPES OF REPORTS

(1) DTNSRDC REPORTS, A FORMAL SERIES PUBLISHING INFORMATION OF PERMANENT TECHNICAL VALUE, DESIGNATED BY A SERIAL REPORT NUMBER.

(2) DEPARTMENTAL REPORTS, A SEMIFORMAL SERIES, RECORDING INFORMATION OF A PRELIMINARY OR TEMPORARY NATURE, OR OF LIMITED INTEREST OR SIGNIFICANCE, CARRYING A DEPARTMENTAL ALPHANUMERIC IDENTIFICATION.

(3) TECHNICAL MEMORANDA, AN INFORMAL SERIES, USUALLY INTERNAL WORKING PAPERS OR DIRECT REPORTS TO SPONSORS, NUMBERED AS TM SERIES REPORTS; NOT FOR GENERAL DISTRIBUTION.

3b (Rev. 11-75)
GPO 928-108

UNCLASSIFIED

SECURITY CLASSIFICATION OF THIS PAGE (When Data Entered)

REPORT DOCUMENTATION PAGE

READ INSTRUCTIONS BEFORE COMPLETING FORM

1. REPORT NUMBER: DTNSRDC Report-76-0051
2. GOVT ACCESSION NO.
3. RECIPIENT'S CATALOG NUMBER

4. TITLE (and Subtitle): EFFECTS OF BOUNDARY-LAYER DEVELOPMENT ON CAVITATION NOISE AND INCEPTION ON A HYDROFOIL.

5. TYPE OF REPORT & PERIOD COVERED: Formal report.

6. PERFORMING ORG. REPORT NUMBER

7. AUTHOR(s): William K. Blake, Melvin J. Wolpert, III, Frank E. Geib, Jr. and Henry T. Wang

8. CONTRACT OR GRANT NUMBER(s)

9. PERFORMING ORGANIZATION NAME AND ADDRESS
David W. Taylor Naval Ship Research and Development Center
Bethesda, Maryland 20084

10. PROGRAM ELEMENT, PROJECT, TASK AREA & WORK UNIT NUMBERS
(See reverse side)

11. CONTROLLING OFFICE NAME AND ADDRESS
David W. Taylor Naval Ship Research and Development Center
Bethesda, Maryland 20084

12. REPORT DATE: December 1976

13. NUMBER OF PAGES: 70

14. MONITORING AGENCY NAME & ADDRESS (if different from Controlling Office)
12 67p.

15. SECURITY CLASS. (of this report): UNCLASSIFIED

15a. DECLASSIFICATION/DOWNGRADING SCHEDULE

16. DISTRIBUTION STATEMENT (of this Report)
APPROVED FOR PUBLIC RELEASE: DISTRIBUTION UNLIMITED

17. DISTRIBUTION STATEMENT (of the abstract entered in Block 20, if different from Report)
16 R01108 17 ZR01108 01

18. SUPPLEMENTARY NOTES

19. KEY WORDS (Continue on reverse side if necessary and identify by block number)
Cavitation
Noise
Cavitation Noise
Cavitation Inception
Boundary Layer

20. ABSTRACT (Continue on reverse side if necessary and identify by block number)
Measurements are described of noise from cavitating flow over hydrofoils. The experiments were performed in a variable pressure water tunnel that was acoustically calibrated so that sound power levels could be deduced from the sound measurements. It was partially reverberant in the frequency range of interest.

(Continued on reverse side)

CONT'

DD FORM 1 JAN 73 1473 EDITION OF 1 NOV 65 IS OBSOLETE
S/N 0102-LF-014-6601

UNCLASSIFIED

SECURITY CLASSIFICATION OF THIS PAGE (When Data Entered)

387682 2B

(Block 10)

Subproject ZR-0110801
Work Units 1-1942-083 and 1-1552-818

(Block 20 continued)

Cavitation was generated on the low-pressure side of a hydrofoil in the presence of a separated laminar boundary layer on the one hand and of a fully turbulent attached boundary layer on the other. The turbulent boundary layer was formed downstream of a trip, which was positioned near the leading edge. High-speed photographs show patterns of cavitation obtained in each case. Cavitation was also generated on the high-pressure side at negative angles of attack. The noise is shown to depend on the type of cavitation produced; for each type, dependence on speed and cavitation index has been determined.

TABLE OF CONTENTS

LIST OF FIGURES

Page

LIST OF TABLES

ABSTRACT

Measurements are described of noise from cavitating flow over hydrofoils. The experiments were performed in a variable pressure water tunnel that was acoustically calibrated so that sound power levels could be deduced from the sound measurements. It was partially reverberant in the frequency range of interest.

Cavitation was generated on the low-pressure side of a hydrofoil in the presence of a separated laminar boundary layer on the one hand and of a fully turbulent attached boundary layer on the other. The turbulent boundary layer was formed downstream of a trip which was positioned near the leading edge. High-speed photographs show patterns of cavitation obtained in each case. Cavitation was also generated on the high-pressure side at negative angles of attack. The noise is shown to depend on the type of cavitation produced; for each type, dependence on speed and cavitation index has been determined.

ADMINISTRATIVE INFORMATION

This work was funded by the David W. Taylor Naval Ship Research and Development Center In-House Research Program under Subproject ZR-0110801, Work Units 1-1942-083 and 1-1552-818.

1. INTRODUCTION

Very few quantitative measurements of noise from surface cavitation on hydrofoils have been reported. Often the measurements have been relative to some arbitrary level, and they have not always been supported by observation of additional parameters which may influence interpretation of the data. Factors which can affect this interpretation include acoustic absorption and reverberation in the test chamber, proximity of the receiver to the cavitation, and hydrodynamic factors that control the type, extent, and inception of cavitation.

In the investigation discussed in this report, an effort has been made to provide coincident acoustic and hydrodynamic observations of hydrofoil cavitation. Measurements have been made of the noise from the hydrofoil on which the boundary layer has been either tripped to turbulence

or not tripped to remain laminar. Viscous effects on the types of cavitation existing have been seen to be responsible for differing noise characteristics. In each case the frequency spectra of noise were unlike those of single-bubble cavitation noise at high frequencies.

The report is organized with Section 2 as a description of instrumentation, while Section 3 discusses the hydrodynamic considerations which led to the final choice of hydrofoil. The noncavitating boundary-layer characteristics and the effectiveness of a leading-edge trip in eliminating laminar separation are discussed in Section 4. In Section 5 the measured influences of the boundary layer on the type of cavitation and of free gas on the inception of each type are described and related to recent observations on axisymmetric head forms. In Section 6 the results of high-speed motion photography of the two types of cavitation observed in this study are reviewed. Sections 7 and 8 are concerned with the noise of each type and with the scaling of traveling bubble cavitation noise.

2. DESCRIPTION OF FOIL AND EXPERIMENTAL TECHNIQUES

GENERAL CONSIDERATIONS

Cavitation measurements of a hydrofoil have been carried out in the David W. Taylor Naval Ship Research and Development Center (DTNSRDC; the Center) 12-in. (30 cm) variable pressure water tunnel, which is open jet and is equipped with a deaeration system but not a resorber. A description of the hydrofoil is given in Section 3. It had a chord of 4 in. (10 cm) and a geometric aspect ratio of 3:1 in the open jet. The brass hydrofoil spanned the test section horizontally and was supported by stainless steel bars which penetrated the tunnel viewing ports; its angle of attack was continually variable. The free-stream water pressure was measured with a closed-end mercury manometer connected to the static pressure tap of a pitot-static tube mounted approximately 3 in. (7.6 cm) above the hydrofoil; see Figure 1. Water temperature was monitored on a thermometer immersed in the test section. Air content was measured by

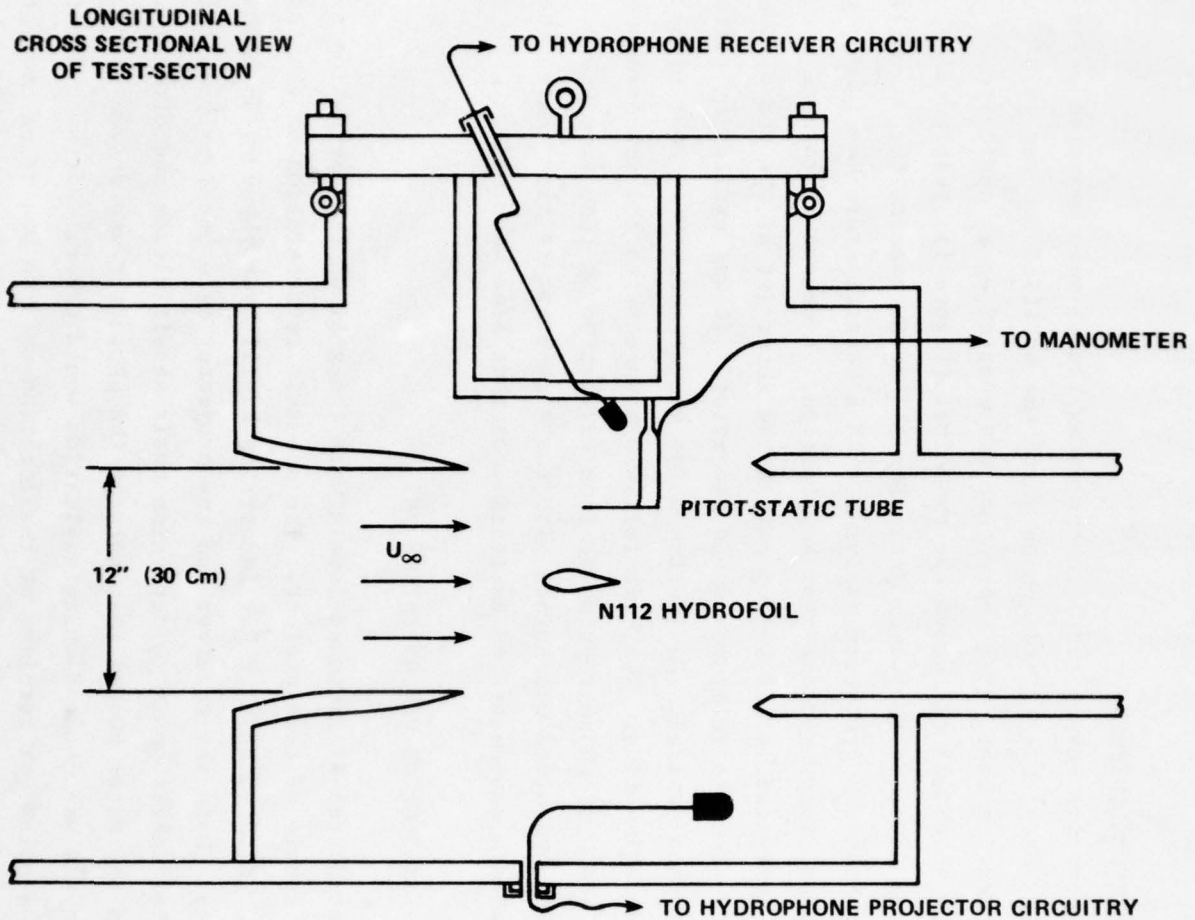

Figure 1 - Experimental Arrangement in the 12-Inch (30 Cm) Variable Pressure Water Tunnel

means of a Yellow Springs Instrument Company "Dissolved Oxygen Meter," Model 51A, as well as with the van Slyke blood-gas apparatus. Air content readings obtained with the dissolved oxygen meter were within 1 percent of those measured with the van Slyke apparatus.

NOISE-MEASUREMENT EQUIPMENT

Sound pressure levels (SPL) in the water tunnel were measured using a KSP Industries Model UT-112 hydrophone which was modified for use in a low-pressure environment. The hydrophone was mounted on an angle iron support about 9 in. (23 cm) above the hydrofoil (Figure 1), just outside the free shear layer of the water jet. For all measurements, the amplified hydrophone output was frequency analyzed with a General Radio Model 1925-1926, 1/3-octave-band filter and detector combination. A second hydrophone was permanently installed in the tunnel out of the water jet at the end of the hydrofoil for use as a reference sound projector. It was excited by filtered random noise when desired. Cavitation noise measurements were made with a 32-second averaging time. The hydrofoil was mounted with the low-pressure side facing the hydrophone when noise from cavitation on that side was being measured. The hydrofoil was turned with the high-pressure side facing the hydrophone when measurements of cavitation on that side were made.

EFFECTS OF TEST SECTION REVERBERATION AND ABSORPTION

Estimated free-field sound levels were the goal of the cavitation noise measurement scheme of this project. The acoustic reverberation of the test section was evaluated using a KSP Industries UT-111 hydrophone as an acoustic volume source. Both the receiver and the projector were previously calibrated in a free-field environment to determine their sensitivities and directivity factors. In the water tunnel test section the projector was driven with random noise and was located where cavitation would occur. For each location, the broadband noise was received at the location used in measuring cavitation

noise. This was a distance of 9 in. (23 cm) above the suction side of the hydrofoil. The ratio of the measurements in the water tunnel to those taken in the free field at a 1-yd (0.9 m) acoustic range gave the corrections to be applied to all cavitation noise measurements so that 1-yd (0.9 m) source levels could be estimated. Actually the measurements were made within one acoustic wavelength of the hydrofoil for frequencies less than 6000 Hz. The procedure used in the reverberation investigation was expected to account for corrections due to any tunnel acoustic resonances which might have existed. Figure 2 shows ratios of sound levels measured in the tunnel at a 9-in. (23 cm) source-receiver separation to the free-field source levels measured at 1-yd (0.9 m) separation. These ratios were used to calculate the effective free-field cavitation noise levels reported in this paper. These levels are approximate for frequencies less than 6000 Hz.

Radiation due to the resonant model excitation of the hydrofoil by the cavitation was investigated. This was accomplished indirectly by mechanically shaking the hydrofoil and measuring the acceleration levels on the foil along with the received acoustic levels at the hydrophone produced by the vibration. A transfer function was obtained which consisted of frequency-dependent ratios of radiated sound level to acceleration averaged over the hydrofoil surface. These measurements will be described in Section 6.

The hydrophone projector mounted out of the flow at one end of the hydrofoil during noise measurements was used to check the acoustic absorption caused by free-gas bubbles. Absorption was detected by measuring the degradation in levels at the receiving hydrophone caused by gas bubbles flowing in the water tunnel which affected both the direct-path and the reverberant sound levels. The investigations indicated that absorption effects would always be less than 1 to 2 dB when no gas bubbles were visible to the unaided eye. Nevertheless, visual observations were frequently supplemented by acoustic observations to insure the quality of the data. The projector was capable of producing noise levels exceeding those generated by the cavitation.

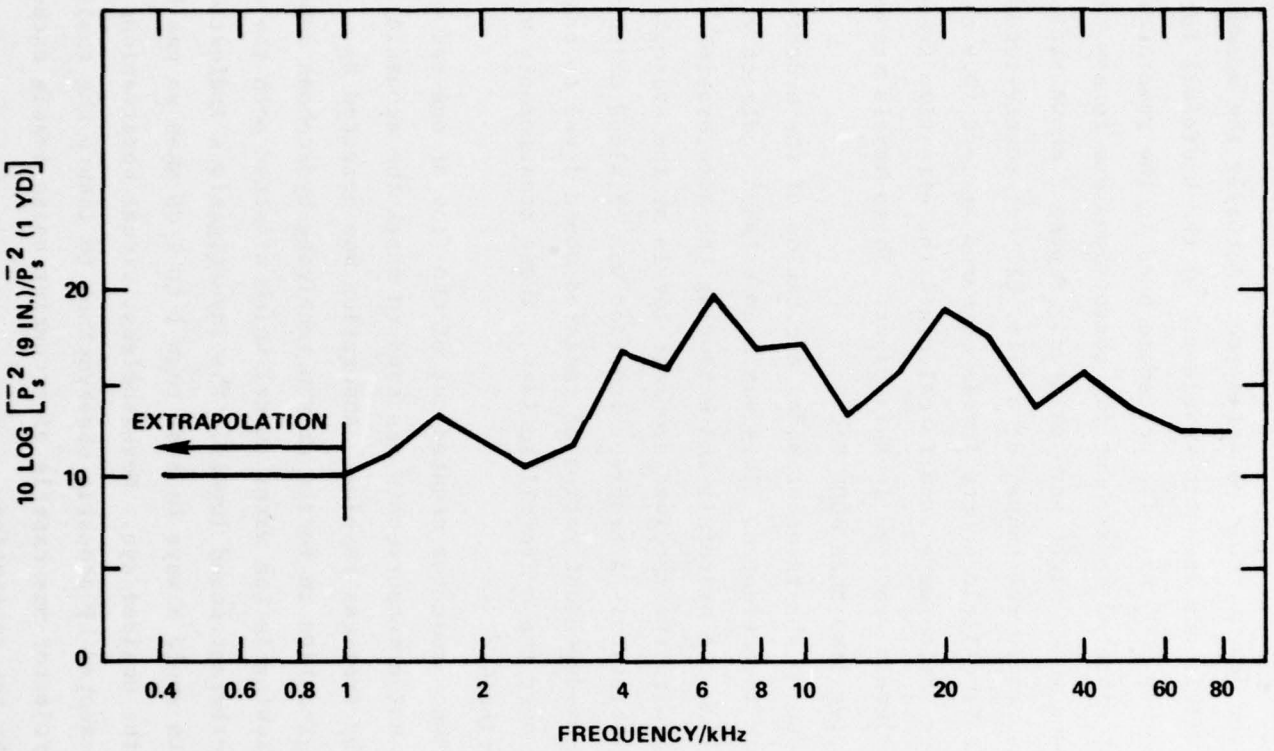

Figure 2 - Test Section Acoustic Calibration, Expressed as Ratio of Mean-Square Pressures, 9 Inches (23 Cm) from Source in Tunnel to that Measured at 1 Yard (0.9 M) in a Free Field

CAVITATION NOISE-MEASUREMENT TECHNIQUES

The measurement procedure involved establishing the tunnel speed for a given run, then reducing the pressure until inception was reached. The noise measurements were then conducted at continually reduced cavitation indices ranging from slightly greater than that for inception to that required for the jet shear layer and/or collector ring to cavitate excessively or until free-gas bubbles were observed. An acoustic absorption from the source of 1 dB usually marked the end of a test. There was no measurable acoustic absorption in the tunnel due to cavitation occurring on the hydrofoil. Background levels were continuously monitored during the experiments by changing the angle of attack of the hydrofoil while maintaining a fixed cavitation index; this change reduced or eliminated the cavitation on the hydrofoil. In another measurement, noise was determined with the hydrofoil removed at a given free-stream cavitation index and water velocity. Background levels were found to be dominated by impeller cavitation for cavitation indices greater than 0.6 and by cavitation in the shear layer of the water tunnel jet for indices less than 0.6. Background levels originating from both of these types of cavitation were somewhat variable. Thus the continuous monitoring of backgrounds as described previously was important.

3. HYDROFOIL SECTION SHAPE AND THEORETICAL PRESSURE DISTRIBUTIONS

The need to simultaneously satisfy the various visual, photographic, and acoustic objectives of the present investigation placed a number of stringent requirements on the hydrofoil section shape. It was desired that the minimum value of pressure coefficient (C_p) on the hydrofoil be as negative as possible so as to obtain cavitation at as high a tunnel pressure and as low a tunnel speed as possible. This would minimize tunnel self-noise and facilitate the acoustic measurements of cavitation. Second, it was desirable to have a relatively large low-pressure region so as to maximize the area of cavitation, to facilitate both acoustic and visual observations

of cavitation. Third, it was desired that the leading portion of the foil have a positive or small negative value of C_p to enable the placement of tripping devices ahead of the cavitation region.

At first, a number of standard NACA (National Advisory Committee for Aeronautics) airfoils were studied. No airfoil in this family was found which simultaneously satisfied the previously described requirements. A further search of airfoil literature revealed that a high-lift Liebeck airfoil[1] (patent pending) at an off-design angle of attack satisfactorily met all of the above requirements. These airfoils are normally used to achieve very high lift coefficients. Their shapes are characterized by a blunt leading edge and a thin trailing edge. At the design angle of attack, these airfoils typically have a fairly flat minimum pressure region which extends from the leading edge to approximately 20 or 30 percent of chord. At lower angles of attack, the minimum pressure region shifts aft. In particular, Figure 14 of Reference 1 shows that Liebeck Airfoil a at an an angle of attack of 4 deg has a pressure distribution which has the characteristics of the desired type. Perhaps the principal drawback of Airfoil a is that it cannot operate at angles of attack less than 4 deg without having separation occur on its pressure side.

As a result, a new Liebeck airfoil shape was designed* which could operate at lower angles of attack. This shape, designated "Airfoil N112," is shown in Figure 3; it has a thickness-to-chord ratio of 18 percent and a camber-to-chord ratio of 3.5 percent. The maximum thickness and camber are located approximately 25 percent of chord aft of the leading edge. The two-dimensional pressure distribution is shown in Figure 4 for an angle of attack α of 4 deg, for which most of the results of the present report were obtained.

---

[1] Liebeck, R.H., "A Class of Airfoils Designed for High Lift in Incompressible Flow," Journal of Aircraft, v. 10, No. 10, pp. 610-617 (Oct 1973). A complete listing of references is given on pages 57 to 59.

*The airfoil was designed according to specified pressure characteristics by Dr. Robert H. Liebeck of the McDonnell Douglas Corporation.

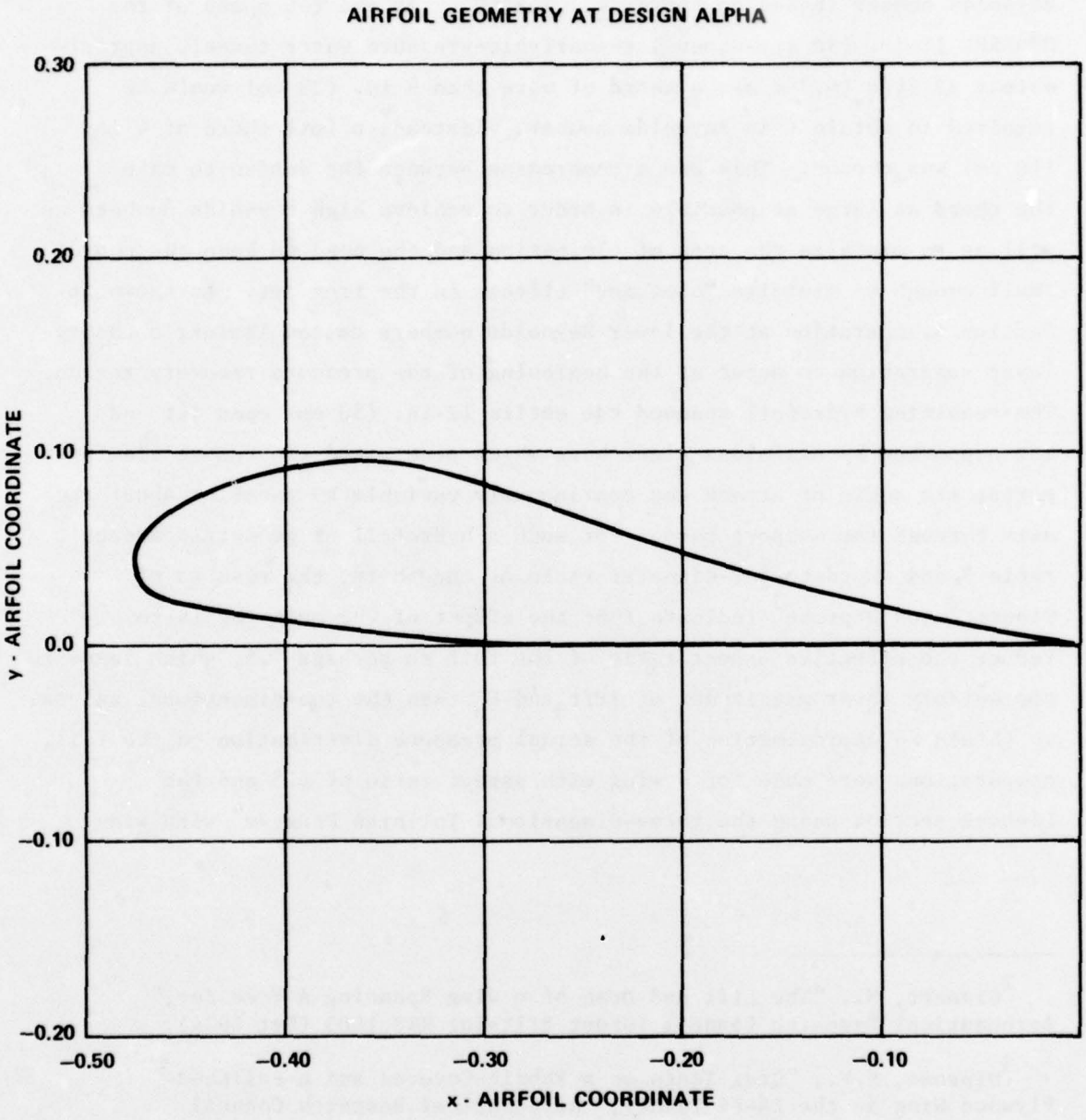

Figure 3 - High-Lift Liebeck Airfoil Shape N112*

*(Patent pending)

The foil was designed to have a two-dimensional pressure distribution so that turbulent separation would, theoretically, be avoided along the entire pressure recovery region on the suction side for $\alpha \leq 5.49$ deg and Reynolds number (based on chord) $\geq 1.7 \times 10^6$. At the top speed of the DTNSRDC 12-in. (30 cm)--open-jet--variable-pressure water tunnel, approximately 22 ft/s (6.7 m/s), a chord of more than 9 in. (23 cm) would be required to obtain this Reynolds number. Instead, a foil chord of 4 in. (10 cm) was chosen. This was a compromise between the desire to make the chord as large as possible in order to achieve high Reynolds numbers as well as to maximize the area of cavitation and the need to keep the chord small enough to minimize "blockage" effects in the free jet. As shown in Section 4, operation at the lower Reynolds numbers caused laminar boundary-layer separation to occur at the beginning of the pressure recovery region. The resulting hydrofoil spanned the entire 12-in. (30 cm) open jet and was supported by stainless steel bars which penetrated the tunnel viewing ports; its angle of attack was continuously variable by rotation about the axis through the support bars. For such a hydrofoil of geometric aspect ratio 3 and chord-to-jet-diameter ratio of one-third, the results of Glauert[2] and Diprose[3] indicate that the effect of the open jet is to reduce the effective aspect ratio of the foil to perhaps 1.5, which leads to appreciably lower magnitudes of lift and C_p than the two-dimensional values. To obtain an approximation of the actual pressure distribution on the foil, computations were made for a wing with aspect ratio of 1.5 and the Liebeck section using the three-dimensional Tulinius Program[4] with wing

---

[2]Glauert, H., "The Lift and Drag of a Wing Spanning A Free Jet," Aeronautical Research Council (Great Britain) R&M 1603 (Mar 1934).

[3]Diprose, K.V., "Drag Tests on a Fabric-Covered and a Polished-Plywood Wing in the 24-Ft Tunnel," Aeronautical Research Council (Great Britain) R&M 1813 (Mar 1937).

[4]Tulinius, J.R., "Theoretical Prediction of Wing-Fuselage Aerodynamic Characteristics at Subsonic Speeds," North American Rockwell Corporation Report NA-69-789 (1969).

thickness effects.[5] This program has been extensively evaluated and has been found to have satisfactory accuracy for most cases.[6] The computed three-dimensional pressure distribution at midspan for a geometric angle of attack of 4 deg is given in Figure 4, which shows the substantial decrease in the magnitude of C_p in the low-pressure region.

The two-dimensional results were obtained by representing the foil section contour by 200 points while only 40 points were used to represent the foil section for the three-dimensional wing due to the larger computer times required for this case. For high-lift Liebeck airfoils, which are characterized by a long thin trailing edge, using a method similar to that of Tulinius and 40 points to represent the foil contour results both in C_p's which have lower magnitudes than the exact values and also in some crossings of the suction side and pressure side C_p's near the trailing edge.* Such crossings were observed for the three-dimensional results over the trailing 20 to 30 percent of the chord.

4. MEASURED PRESSURE DISTRIBUTIONS AND BOUNDARY LAYERS ON THE HYDROFOIL

Our comments will be restricted to cavitation on the suction or low-pressure side of the hydrofoil. The static pressure distribution was determined by using static pressure taps at locations downstream of the leading edge at 7.5, 20, 30, and 40 percent of the chord (c). Figure 4 shows the section shape and the 2-D and 3-D theoretical and measured pressure distributions at a 4-deg angle of attack. Measurements are shown as a function of speed for the tripped boundary layer and at a single

---

[5] Tulinius, J.R., "Theoretical Prediction of Thick Wing Aerodynamic Characteristics at Subsonic Speeds," North American Rockwell Corporation Report NA-70-104 (Oct 1970).

[6] Wang, H.T., "Comprehensive Evaluation of Six Thin-Wing, Lifting-Surface Computer Programs," NSRDC Report 4333 (Jun 1974).

* Private communication from Dr. R.H. Liebeck of the McDonnell Douglas Corporation.

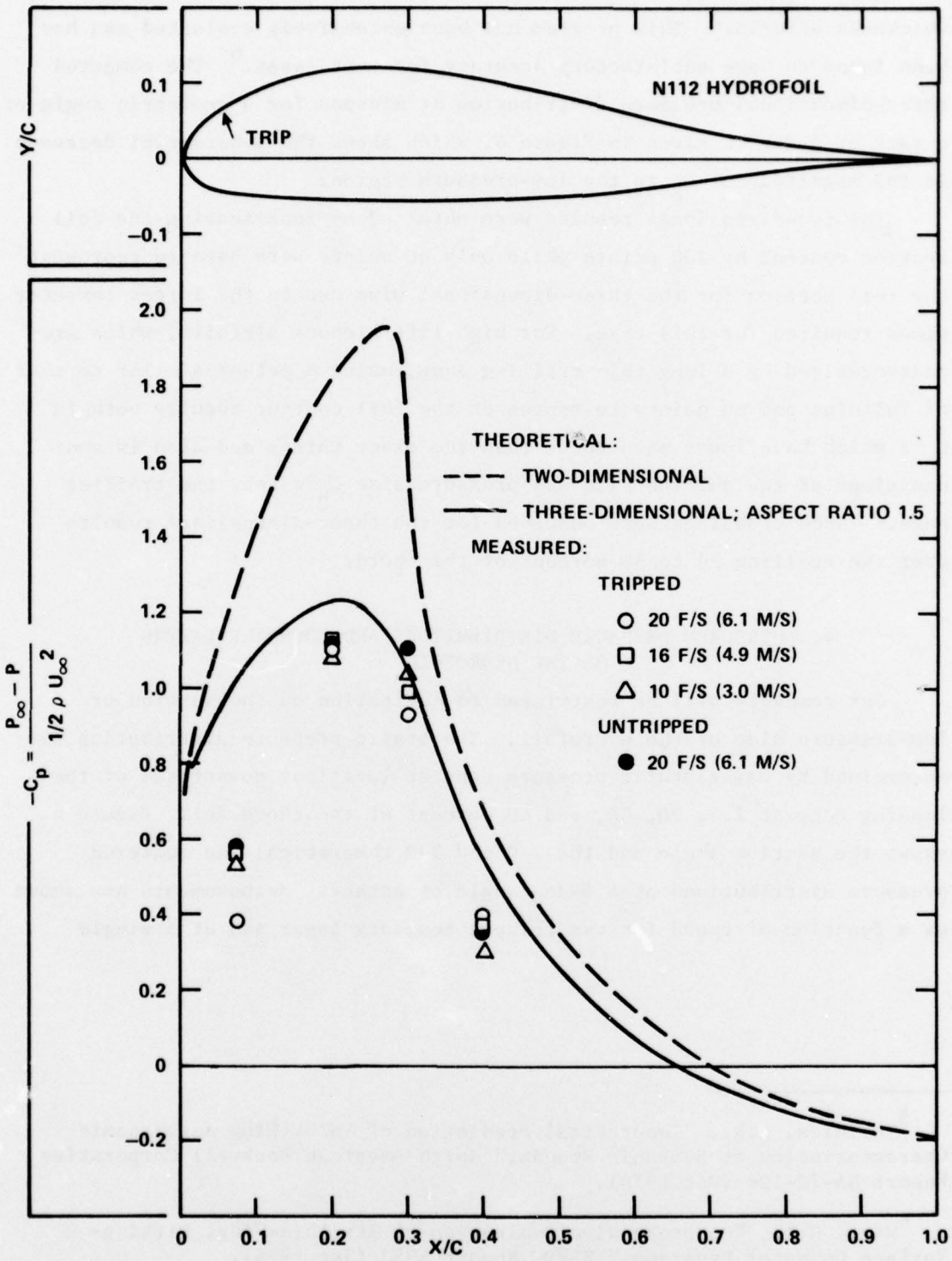

Figure 4 - Pressure Coefficients and Cross Section Shape of Liebeck N112 Hydrofoil
(Data and theoretical calculations are for 4-degree angle of attack with tripped and untripped boundary layers on the suction side)

speed without the trip. The coefficients give local pressures (P) relative to the ambient static pressure (P_∞) normalized on the inflow speed (U_∞). Laminar boundary-layer separation was experimentally established for non-tripped flow by using an oil film experiment. A mixture of lampblack and high-viscosity (SAE 90) gear oil was applied to the suction side of the hydrofoil; the tunnel was then filled, and the water was accelerated to a selected speed. The region of separation was indicated by a band of oil which remained on the hydrofoil surface. Table 1 shows the extent of the separation at a 4-deg angle of attack for six speeds. The spatial resolution of the oil film was within 1/16 in. (0.16 cm). At 6 ft/s (1.8 m/s) the separation extended to the trailing edge. From 15 to 22 ft/s (4.6 to 6.7 m/s) it was of small chordwise extent, and it was uniform along the entire span. At 25 ft/s (7.6 m/s) the chordwise extent was only about 0.1 in. (0.25 cm) and it occurred in a broken line along the span. Patterns of similar chordwise and spanwise extent were observed at α = 2 degrees.

That the free-stream turbulence in the water tunnel was insufficient to cause natural transition on the untripped hydrofoil was established by using criteria of *Hall and Gibbings* (1972).[7] The broadband root-mean-square turbulence intensity at the centerline was 2 percent of the free-stream velocity at the centerline. Using the equations for laminar boundary layer growth in the absence of a pressure gradient (Schlichting (1960)[8]), we estimated that the Reynolds number at the observed separation point was only $U_\infty\theta/\nu = 290$. The effect of the favorable pressure gradient would have been to reduce the momentum thickness (θ) as well as to further stabilize the laminar boundary layer. Without the stabilizing influence of the pressure gradient, Hall and Gibbings[7] showed that the Reynolds number required for transition with a freestream turbulence intensity of 1.5 percent was at least $U_\infty\theta/\nu = 400$.

---

[7]Hall, D.J. and J.C. Gibbings, "The Influence of Stream Turbulence and Pressure Gradient upon Boundary Layer Transition," Journal of Mechanical Engineering Science, v. 14, pp. 134-146 (1972).

[8]Schlichting, H., "Boundary Layer Theory," McGraw-Hill, Inc. (1960).

TABLE 1 - SEPARATION REGION ON HIGH-LIFTING HYDROFOILS

Inflow Speed in feet per second:	m/sec	Region of Separation α = 4 deg
6	(1.8).....	$0.25 < x/c < 1$
8	(2.4).....	$0.25 < x/c < 0.55$ to 0.75
15	(4.6).....	$0.28 < x/c < 0.35$
20	(6.1).....	$\sim 0.3 < x/c < \sim 0.33$
22	(6.7).....	$0.3 < x/c < 0.33$
24	(7.3).....	$0.3 < x/c < 0.33$

The boundary-layer trip was a strip of tape 1/32-in. (0.08 cm) in streamwise extent with a height of 5.6×10^{-3} in. (14×10^{-3} cm). The trailing edge of the trip was situated approximately at $x/c = 0.04$. The trip was designed by determining that the estimated height of the laminar boundary layer at the trip location, which was 4.3×10^{-3} in. (11×10^{-3} cm) at 22 ft/s (6.7 m/s), was less than the height of the trip. Its effectiveness was speed dependent. The oil-film experiment disclosed that laminar separation at $\alpha = 4$ deg and 16 ft/s (4.9 m/s) was intermittent as deduced by the rapid occurrence of a fairly well-defined oil accumulation which gradually washed off. At higher speeds no separation could be detected on the suction side of the hydrofoil, indicating that transition to turbulence occurred upstream of the position of minimum pressure. The static pressure distributions (Figure 4) reflect speed dependence for effectiveness of the trip in eliminating the separation. At $x/c = 0.2$ the pressure coefficients are independent of speed; at $x/c = 0.3$ the pressure coefficients for the tripped boundary layer consistently approached the pressure coefficient for the untripped laminar boundary layer as the speed was reduced.

Measured static pressure distributions on the hydrofoil at other angles of attack are shown in Figure 5. As the angle of attack increased beyond $\alpha = 0$ deg, the influence of the boundary-layer separation became more important. The dotted lines in the figure are estimated pressure curves.

5. CHARACTERISTICS OF CAVITATION INCEPTION

CAVITATION INCEPTION

This section examines the influence of the boundary layer on the type of cavitation that developed on the hydrofoil as well as some effects of undissolved gas in the free stream on the inception of each type of cavitation. Incipient cavitation indices were determined by slowly lowering the tunnel pressure at constant water velocity until fully developed cavitation occurred. Definition of the onset depended on each type of cavitation that occurred. Desinent indices were

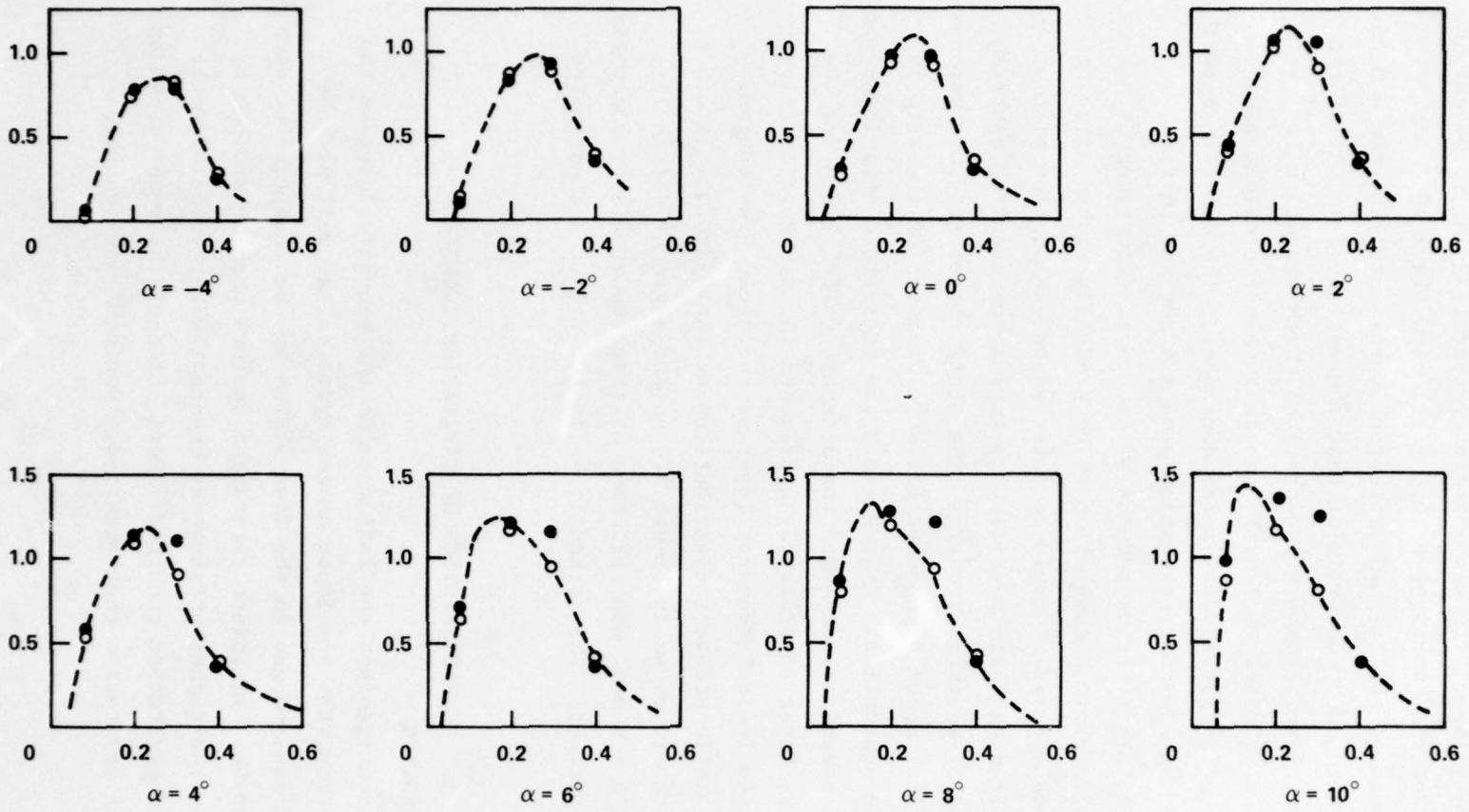

Figure 5 - Static Pressure Distributions for High-Lift Foil for various Angles of Incidence for Trippedoand Untripped●Boundary Layers, U_∞ = 20 Ft/S (6.1 M/S)

(Vertical scale is $-C_p$ and horizontal scale is x/c)

determined by increasing the static pressure and noting the cessation of cavitation. In all cases the cavitation has been characterized by the index

$$\sigma = \frac{P_\infty - P_v}{1/2\ \rho\ U_\infty^2}$$

where p_v is the vapor pressure of water.
The incipient indices are denoted by σ_i and the desinent indices by σ_d. All measurements were performed with dissolved air contents on the order of 1 to 2.4 ppmw (parts per million, weight), corresponding to 5 to 12 percent of saturation at the measured water temperature and atmospheric pressure. Free-gas content, detected by acoustic absorption, was observed to increase slightly with time after filling. Although no direct quantitative dependence of σ_i on dissolved air content could be determined, inception indices increased slightly with time after filling.

EFFECTS OF BOUNDARY-LAYER TRIPPING ON CAVITATION ON LOW-PRESSURE SIDE

Cavitation which incepted in the vicinity of the separated laminar boundary layer, i.e., with no trip, appeared as a well-defined strip which extended chordwise downstream from $x/c \simeq 0.25$. Figure 6 shows typical views of this type of cavitation, photographed under stroboscopic light with a duration of 3×10^{-3} seconds. The forward edge of the cavitation is smooth in spots, indicating nonturbulent flow at those locations. Downstream of the forward edge, the cavity is broken up; however, the high density of bubbles is still well defined in its chordwise extent. Visual observation of the cavitation showed that the approximate chordwise length of the cavitation region (ℓ_c) appeared to be roughly proportional to ($\sigma_i - \sigma$). Further discussion of these photographs will be given in the next section.

Figure 6a

Figure 6b

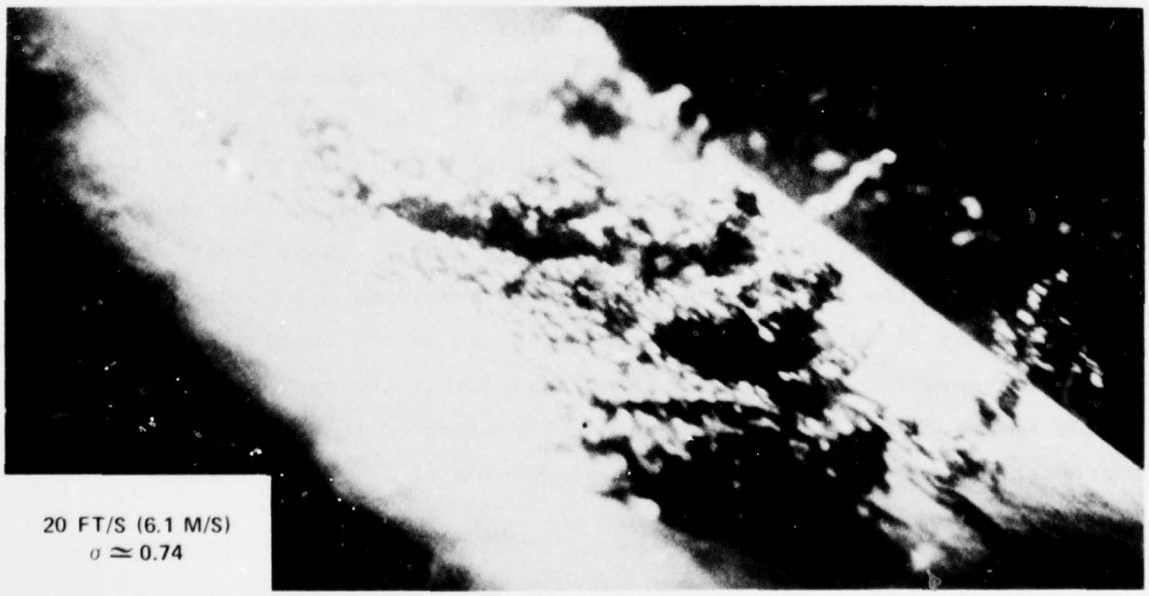

Figure 6c

Figure 6 - Representative Cavitation without Boundary-Layer Tripping for $\sigma \simeq 1.15$ with U_∞ = 16 Ft/S (4.9 M/S) and $\sigma \simeq 0.74$ with U_∞ = 20 Ft/S (6.1 M/S)

Incipient and desinent indices are shown in Figure 7. Inception was defined visually when cavitation was unsteady but was present on the hydrofoil 50 to 80 percent of the time. The data are typical of the 16- to 22-ft/s (4.9- to 6.7-m/s) speed range. The flagged and nonflagged points were obtained on different days, separated by tunnel drainings and fillings. For the flagged points, there was no acoustic absorption from the reference source, while for the nonflagged points, absorption of 1 to 2 dB occurred in the 10- to 100-kHz frequency range. The dotted line in Figure 7 shows the dependence of the measured minimum pressure coefficient with angle of attack. Actual minima may have been as much as 10 percent lower than the ones measured because the wide spacing of the static pressure taps may not have been sufficient to resolve the pressure distribution accurately. This has been indicated in Figure 5.

When cavitation incepted on the hydrofoil in the vicinity of an attached (tripped) turbulent boundary layer, the visual appearance of the cavitation was that of white streaks passing over the region of low pressure on the hydrofoil, roughly from $0.15 < x/c < 0.90$. Figure 8 is a stroboscopic photograph of this cavitation at $\sigma = 0.78$, showing that the white streaks were comprised of discrete bubbles having a wide range of sizes and shapes. These photographs will be further discussed in Section 6. The incipient and desinent indices for this cavitation on the hydrofoil are shown in Figure 9. Inception of this cavitation was detectable as a sequence of clearly distinguishable "events." As static pressure was reduced, the event rate increased. Event counting was accomplished audibly by using a wristwatch while observing the cavitation for 30 seconds. Two sets of incipient indices appear in the figure, these are the results of separate measurements on different days. The first set, denoted by the nonflagged points, was measured during a period when a small air leak in the tunnel brought about a slow accumulation of free gas, causing from 1 to 2 dB absorption as indicated by the reference source. These inception points were established on the basis of the first audible event. The second set of indices was obtained when the

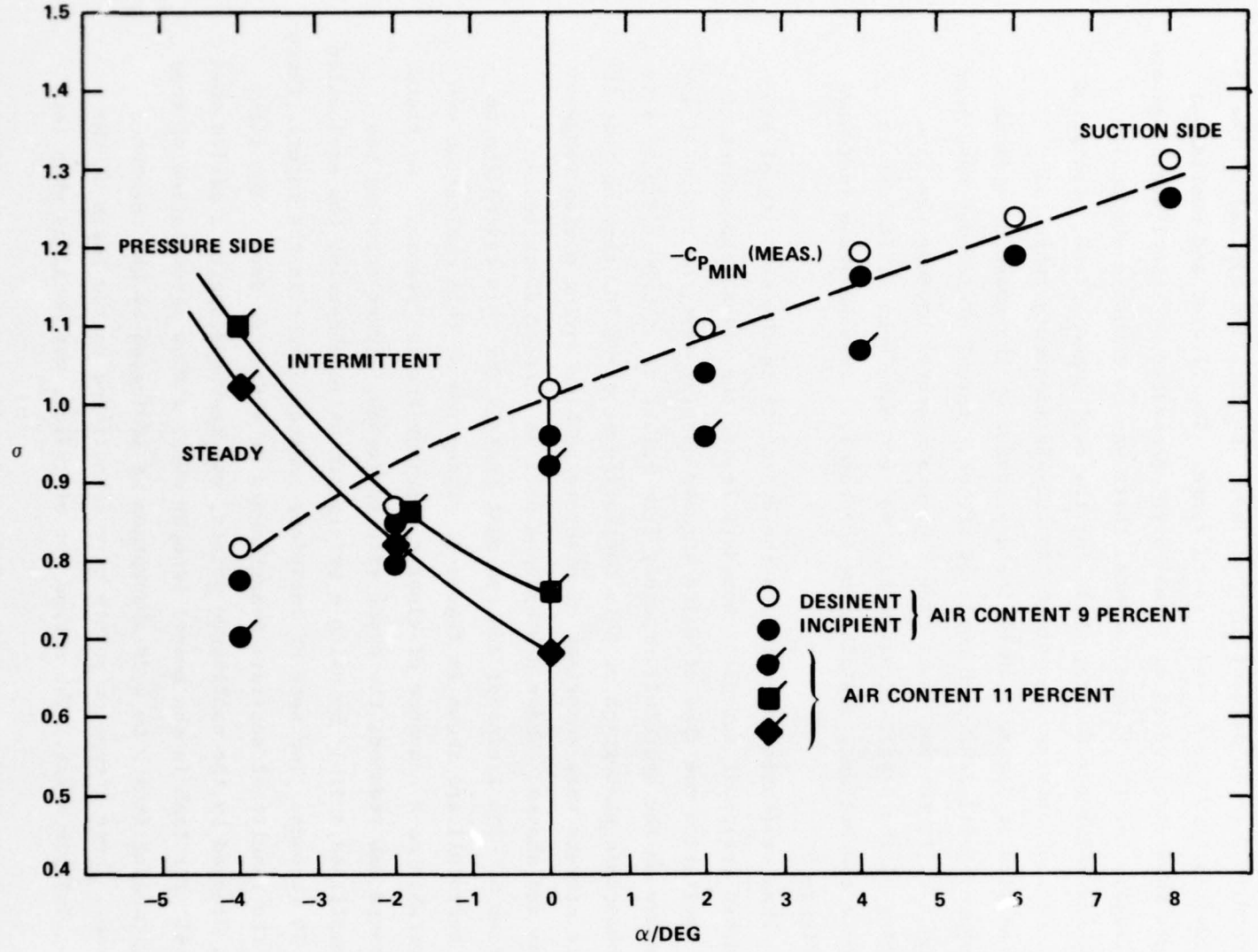

Figure 7 - Incipient and Desinent Cavitation Numbers for Hydrofoil with No Trip, Shown as Function of Angle of Attack for U_∞ = 22 Ft/S (6.70 M/S)

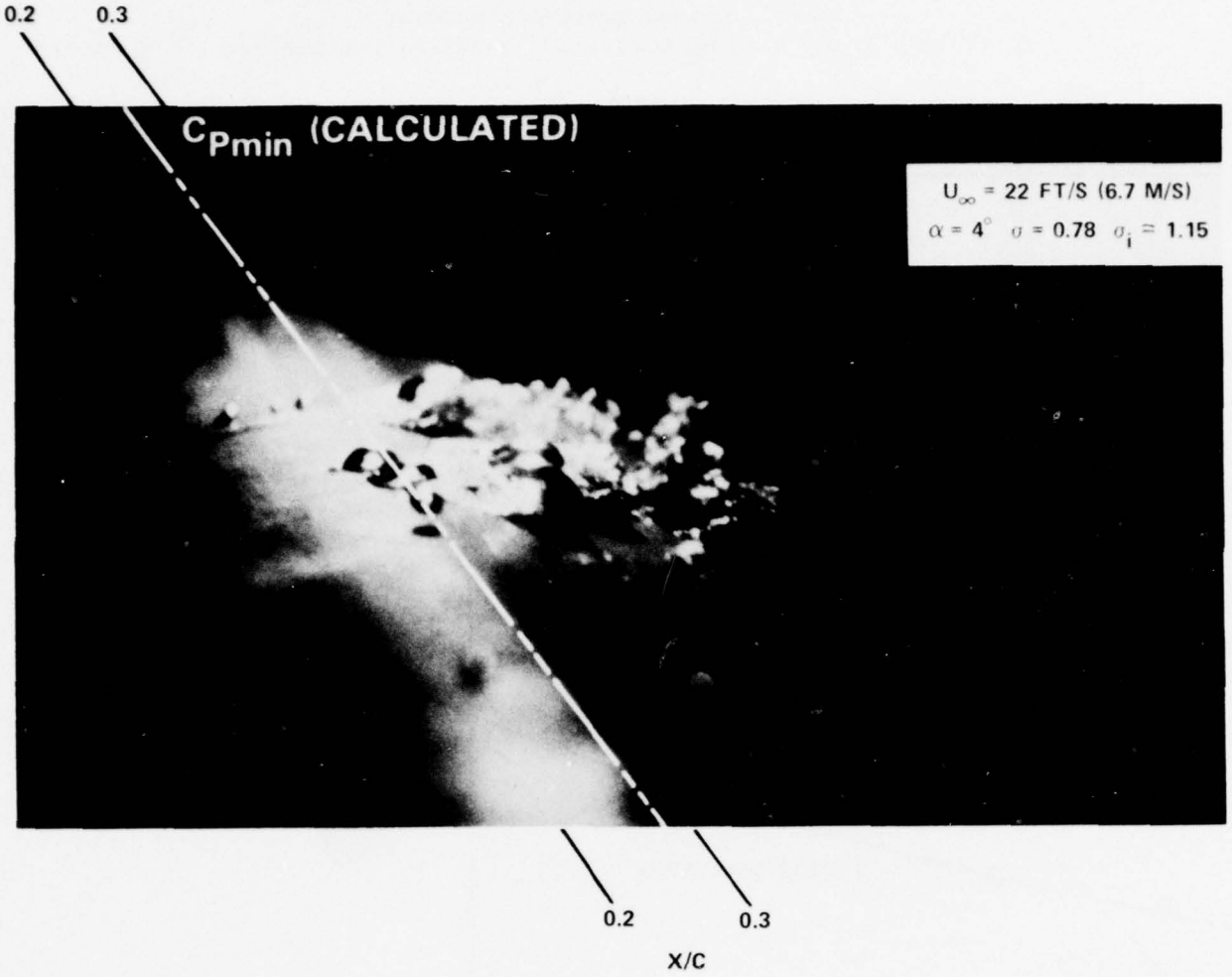

Figure 8 - Traveling Bubble Cavitation Associated with Tripped Turbulent Boundary Layer for U_∞ = 22 Ft/S (6.70 M/S), α = 4 Degrees, σ = 0.78, and σ_i = 1.15

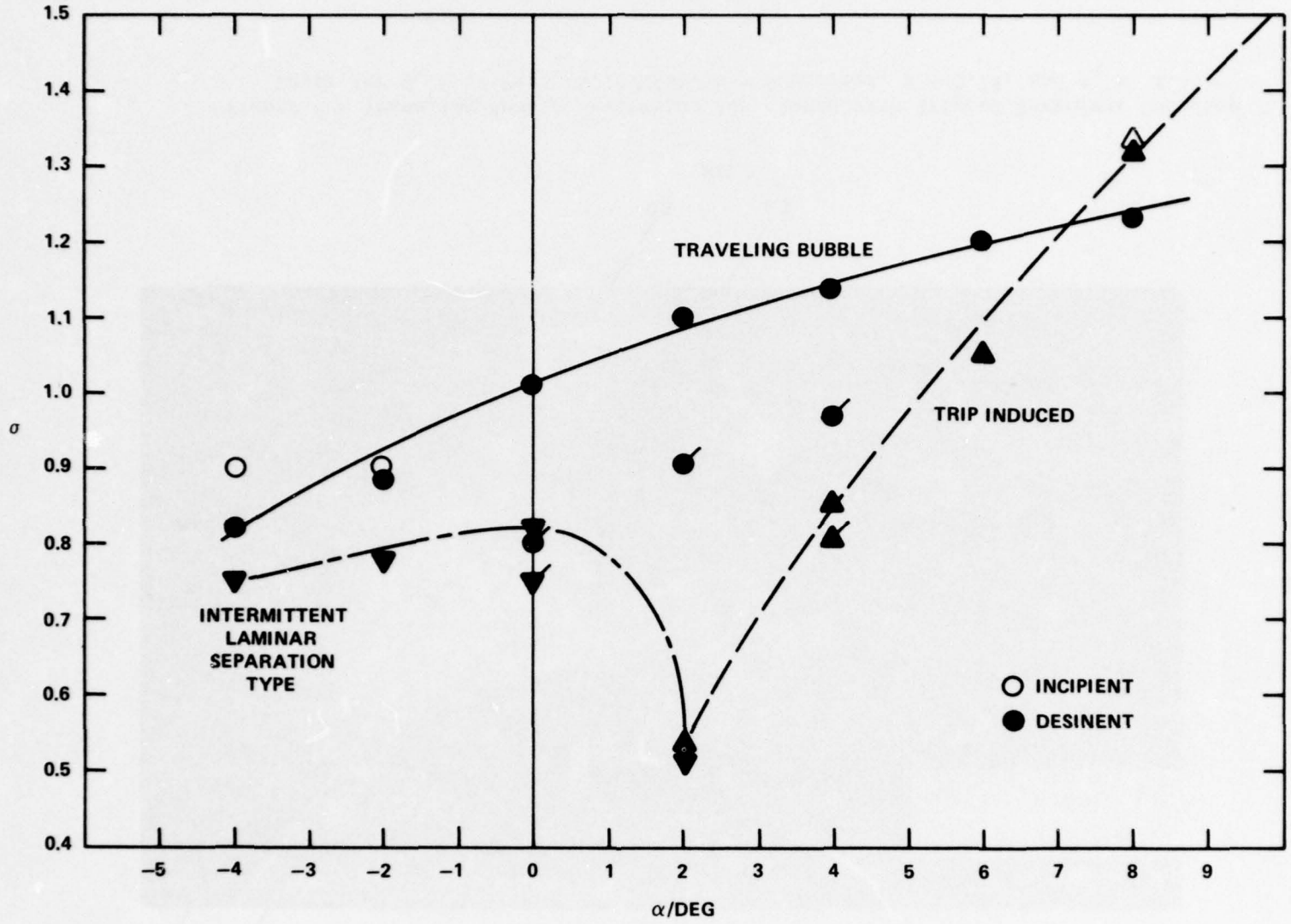

Figure 9 - Incipient and Desinent Cavitation Numbers for Hydrofoil with a Tripped Turbulent Boundary Layer
(Inception of cavitation types on suction side are shown for varying quantities of free gas; U_∞ = 22 Ft/S (6.1 M/S)

leak had been repaired, using a steady event rate from 1 to 2 per second. The dissolved air content remained at 8 percent of saturation at tunnel temperature and atmospheric pressure for both measurements. At α = 4 deg, incipient traveling bubble cavitation occurred for σ_i = 1.13.

The uncertainty in σ_i caused by the different event-rate criteria is approximately 6 percent. Further reduction in the static pressure of the tunnel resulted in the first occurrence of trip-induced cavitation at σ = 0.85. At this index the cavitation was very intermittent, occurring at long time intervals and often at one location along the span. This indicated that a slight spatial nonuniformity in the trip shape caused the cavitation. The cavitation of three-dimensional triangular protuberances, which typify local pointed elements on a hydrofoil, has been examined by Holl et al. (1972).[9] Use of the estimated boundary-layer characteristic at the trip location of the present hydrofoil resulted in an estimate of $\sigma_i \approx 0.67$. At larger angles of attack the cavitation of the hydrofoil became totally dominated by the trip. On the other hand for $\alpha < 2$ deg, the trip-induced cavitation became nonexistent; however, an intermittent type, typical of that associated with the laminar separation of the untripped hydrofoil, became apparent. For increasingly negative angles of attack, the cavitation associated with laminar boundary-layer separation soon followed the inception of traveling-bubble cavitation. Apparently the turbulence induced by the trip became stabilized as the stagnation point approached the trip location, allowing the pressure gradient there to become strongly favorable with reduced α. Also, as the local pressure coefficient approached zero the trip-induced cavitation was prevented. Comparisons of σ_i for the cavitation related to laminar separation in Figures 7 and 9 show that at α = -4 deg, the cavitation characteristics

---

[9] Holl, J.W. et al., "Limited Cavitation and the Related Scale Effects Problem," Second International Japanese Society of Mechanical Engineers Symposium (1972).

of the tripped and untripped hydrofoils were comparable. Also note that the differences between σ_i and σ_d are more apparent for the cavitation on the untripped hydrofoil than on the tripped hydrofoil.

CAVITATION ON THE HIGH-PRESSURE SIDE

Incipient indices for the pressure-side cavitation are shown for intermittent and steady cavitation in Figure 7. This cavitation had the visual appearance of a sheet of bubbles which extended from the leading edge and collapsed just above the surface of the hydrofoil. Figure 10 shows high-speed photographs of this cavitation at various stages of development. The surface of the cavity becomes distorted with small-scale ripples very near the leading edge. The unsteadiness of the overall cavity shape at a given value of σ and U_∞ is apparent in the photographs. The cavitation appears as groups of bubbles which are formed in sheets near the leading edge and which persist downstream, collapsing either above or completely downstream of the surface of the hydrofoil.

VISCOUS EFFECTS ON INCEPTION

Viscous effects on the cavitation inception of axisymmetric head forms have been discussed by Peterson (1969)[10] and have been observed by Arakeri and Acosta (1973)[11] and Acosta (1974).[12] When

---

[10]Peterson, F.B., "Water Tunnel--High-Speed Basin Cavitation Inception Comparison," 12th International Towing Tank Conference, pp. 519-523 (1969).

[11]Arakeri, V.H. and A.J. Acosta, "Viscous Effects in the Inception of Cavitation on Axisymmetric Bodies," Journal of Fluids Engineering, American Society of Mechanical Engineers, v. 95, Ser. 1, No. 4, pp. 519-528 (1973).

[12]Acosta, A.J., "Cavitation and Fluid Machinery," Cavitation Conference, Edinburg, Scotland (1974).

Figure 10 - High-Speed Photographs of Cavitation on High-Pressure Side of Hydrofoil; U_∞ = 16 Ft/S (6.1 M/S) α = -2 Degrees

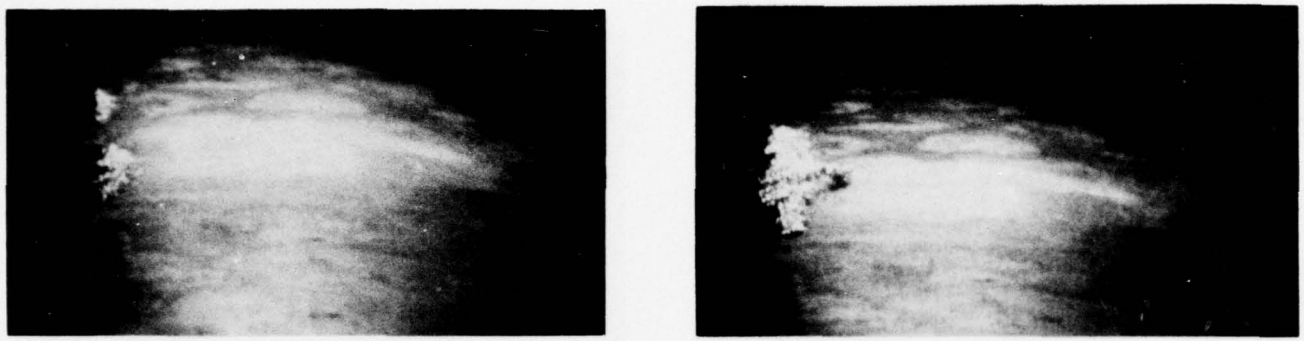

Figure 10a - $\sigma = \sigma_i = 0.98$

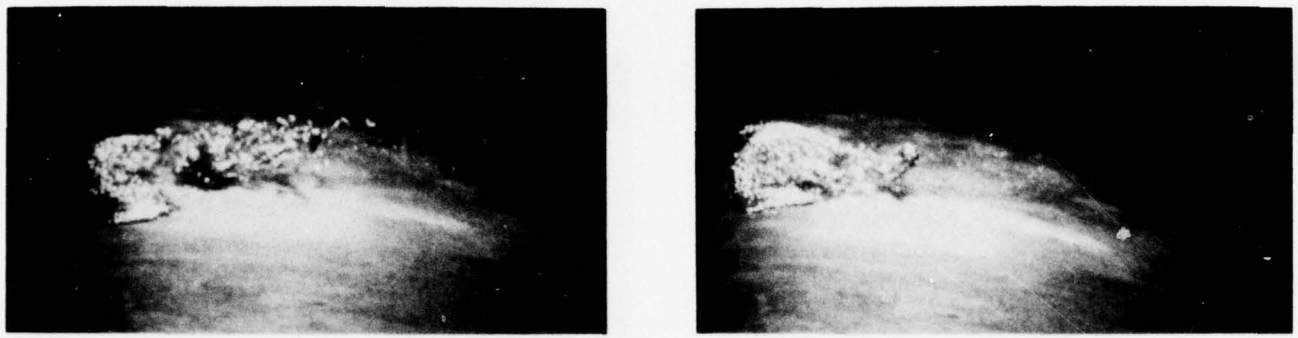

Figure 10b - $\sigma = 0.90$

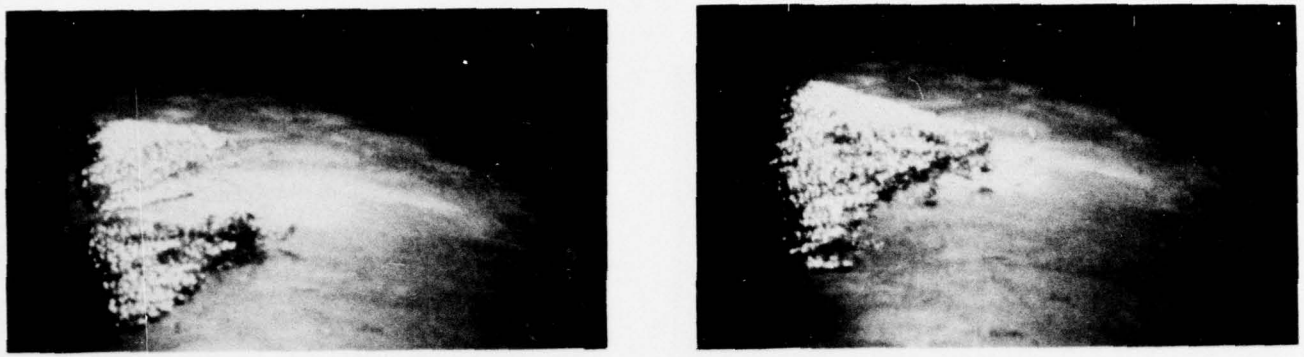

Figure 10c - $\sigma = 0.80$

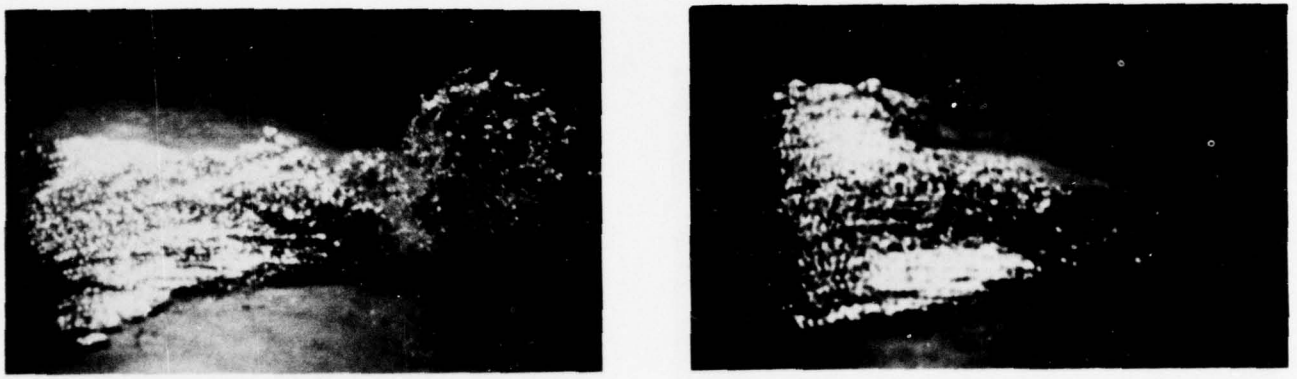

Figure 10d - $\sigma = 0.70$

laminar boundary-layer separation occurs, cavitation has been observed to occur at higher cavitation indices than when separation is prevented. In this connection, Casey (1974)[13] has quantitatively related experimentally observed values of σ_i with computed static pressure coefficients on a hydrofoil at flow separation. He has also correlated the observed location of the cavitation with the observed location of laminar boundary-layer separation. In the current experiments, laminar separation on the low-pressure side occurred slightly downstream of but still near the point of the measured minimum pressure coefficient ($C_{p_{min}}$) and the cavitation was entirely contained downstream of that point. This can be seen in Figure 11, which compares the measured pressure distributions with photographs of the incipient cavitation. The downstream extremity of the region of laminar separation can be seen to coincide with the location of small bubbles. Dynamics of the cavitation as disclosed by the high-speed motion photography described in Section 6 were clearly seen to be initiated by the formation of these small bubbles. Thus, inception occurred at the reattachment point of the separation zone. This is in agreement with the head-form observations of Arakeri and Acosta[11] which showed bubbles to be formed in this region. The generally lower σ_i for the traveling-bubble cavitation on the tripped hydrofoil, compared to the untripped cases, can be seen in Table 2. Well-developed, steady-state bound cavitation occurred at 10 percent higher σ when laminar separation occurred than when it was suppressed by tripping. Data in Table 2 were generated within a single day at the same time as the flagged points of Figures 7 and 9 with a single tunnel filling. These data represent flow situations before and after removal of the trip so they are not influenced by uncertainties caused by time-dependent--free-gas accumulation. The occurrence of the occasional audible events associated with $\sigma > \sigma_i$ for traveling bubbles is most likely due to local pressure fluctuations in the turbulent boundary layer of the hydrofoil which have a small yet nonetheless finite probability of being less than the critical pressure required for

---

[13] Casey, M.V., "The Inception of Attached Cavitation from Laminar Separation Bubbles on Hydrofoils," Cavitation Conference, Edinburg, Scotland (1974).

TABLE 2 - COMPARISON OF TRIPPED VERSUS NONTRIPPED σ_i FOR LIEBECK N112 HYDROFOIL, 2.2 PPMW AIR CONTENT* (1 TO 2 EVENTS PER SECOND)

α deg	U_∞ ft/s	U_∞ m/s	No Trip	Trip	$-C_{p_{min}}$ (meas.)
4	18	(5.5)	1.09	0.90	1.13
4	22	(6.7)	1.02	0.90	1.13
2	22	(6.7)	0.95	0.86	1.05
0	22	(6.7)	0.92	0.80	0.96

*Approximately 11 percent saturation at atmospheric pressure and 75°F (24°C)

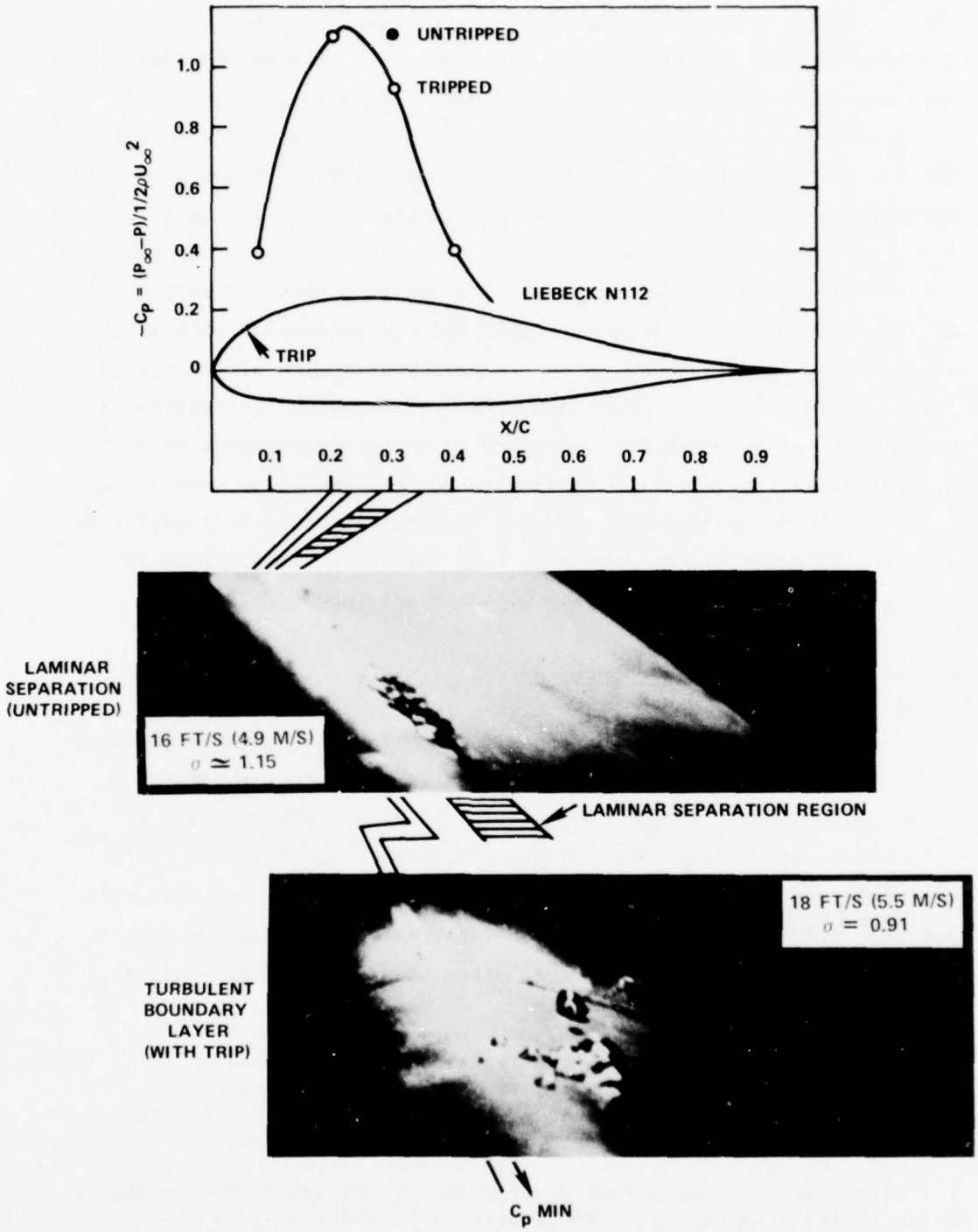

Figure 11 - Pressure Distributions and Cavitation Patterns near Inception as Influenced by Viscous Effects (Photographs were obtained at differing angles to optimize lighting; lines mark coordinates of x/C = 0.2, $C_{p_{min}}$, and observed separation zone)

bubble growth. The cause of inception occurring at higher σ for a case involving laminar separation than for cases with attached boundary-layer flows has been attributed to extraordinarily high wall-pressure fluctuations occurring at the reattachment point of the separation. Arakeri[14] has observed that these fluctuations are considerably higher than when separation is suppressed; broadband fluctuations extending to 10 percent of the dynamic head were observed on a hemispherical nose. In the case of a two-dimensional strut, pressure fluctuations about 18 percent of the free-stream dynamic head were observed (in connection with another experiment, Blake (1975)[15]) in the reattachment region of the separated flow downstream of a circular leading edge. Pressure fluctuations in the fully developed turbulent boundary-layer flow just downstream of the reattachment zone of the separation on the same strut were a factor of 10 less than those associated with the separation. Additional evidence of the role of local pressure (and velocity) fluctuations in causing cavitation has been given by Arndt and Ippen (1967).[16]

SOME EFFECTS OF FREE-GAS CONTENT ON CAVITATION ON LOW-PRESSURE SIDE

Inception indices for the traveling bubble cavitation as shown in Figure 9 differ by about 20 percent. The lower inception indices accompanying lower free-gas content are consistent with results of earlier investigations. For example, Peterson[10] and Brockett (1972)[17] have shown occasional tendencies of σ_i to increase with both gas content and with time after filling the water tunnels without resorbers. The acoustic absorption at 1/5 atm, often observed in this study at

---

[14] Arakeri, V.H., "A Note on the Transition Observations on an Axisymmetric Body and Some Related Fluctuating-Wall Pressure Measurements," Journal of Fluids Engineering, Transactions American Society of Mechanical Engineers, v. 97, Ser. 1, No. 1, pp. 82-86 (1975).

[15] Blake, W.K., "Statistical Description of Pressure and Velocity Fields at Trailing Edges," NSRDC Report 4241 (1975).

[16] Arndt, R.E.A. and A.T. Ippen, "Cavitation Near Surfaces of Distributed Roughness," Massachusetts Institute of Technology Hydrodynamics Laboratory Report 104 (1967).

[17] Brockett, T., "Some Environmental Effects on Headform Cavitation Inception," NSRDC Report 3974 (1972).

50 kHz, required the resonant excitation of suspended bubbles with radii approximately of 3×10^{-3} cm. Although only a 1 to 2 dB absorption in this frequency range was the maximum tolerated for the current measurements, these and smaller bubbles were obviously present in the tunnel. Furthermore, Peterson (1972)[18] has holographically measured stable bubbles with radii of approximately 10^{-3} cm in the same facility but at a slightly higher static pressure than that used in the current measurements. Strasberg (1956)[19] has shown that the critical pressure for cavitation varies as functions of both nucleus bubble radius and free-gas content. Decreasing gas-nucleus (bubble) sizes and decreasing the undissolved concentrations caused a marked decrease in critical pressure. Therefore, it is reasonable to expect that in the current measurements, when no absorption existed at less than 50 kHz, all gas-filled nuclei were less than 10^{-3} cm in radius, and they became available in increasing numbers as the static pressure in the water tunnel was reduced. Since the specific nucleus required for the different types of cavitation is not known, and since both hydrophobic solid and free-bubble particles have been shown by Peterson[18] to exist in the facility, a clear and quantative dependence of σ_i on the free-gas content cannot be assessed.

6. SOME DETAILS OF CAVITATION DYNAMICS DEDUCED FROM HIGH-SPEED MOTION PHOTOGRAPHY

High-speed motion picture photography, with frame rates ranging from 3000 to 8000 fr/s, was used to observe cavitation on the low-pressure side of both the tripped and the nontripped hydrofoil. The cavitation was photographed along the span of the hydrofoil, using backlighting provided by a 2-kw Colostran lamp. The high-speed motion picture camera was a Red Lake Laboratories Hycam model with a 400-ft film capacity and 50-mm Schneider lens. Kodak high-speed Ektachrome (EFB 7242) 16-mm film

---

[18] Peterson, F.B., "Hydrodynamic Cavitation and Some Considerations of the Influence of Free-Gas Content," Ninth Symposium on Naval Hydromechanics, Paris, France (1972).

[19] Strasberg, M., "The Influence of Air-Filled Nuclei on Cavitation Inception," DTMB Report 1078 (1956).

was used for all movies. Both the camera and the lamp were situated outside the water tunnel with viewing through windows of 2-in. (5 cm)-thick, commercial grade Plexiglas. The distance from the inside wall of the tunnel viewing port to the center of the hydrofoil was approximately 13 in. (33 cm). The stroboscopic photographs of Figures 6 and 8 will be used to illustrate descriptions of the filmed observations.

For the untripped hydrofoil near inception, the film disclosed that small bubbles were generated at a location corresponding to the downstream extremity of the laminar separated flow region. Figures 6a and 11, for which $\sigma = \sigma_i \approx 1.15$, show this by the small bubbles of cavitation at the location corresponding to the reattachment point of the separation. Following their formation, the bubbles moved forward toward the location of $C_{p_{min}}$, stopping and joining at the leading edge of the separation zone to form a flattened single bubble which is also shown in Figures 6a and 11. Further generation of bubbles caused spanwise growth of each small bound cavity first along the downstream extremity and then along its leading edge. Eventually these smaller cavity regions joined adjacent ones. Concurrently, the height of the bound cavity as well as its chordwise extent would increase so that the bound cavitation occupied a much larger volume than the original noncavitating flow separation region probably had. Figures 6a and 6b, both obtained at $\sigma = \sigma_i$, show the mirrorlike leading edge of the vapor pocket which was formed from the smaller bubbles. The downstream section of the pocket is broken up probably by turbulence in the liquid flow over it. Also, the larger extent of the fully developed cavity region, compared to the incipient region, is clearly evident. For the more advanced stages of cavitation, exemplified by Figure 6c taken at $\sigma \approx 0.74$, both the height and especially the chordwise length of the cavitation region grew and unsteadiness became apparent. Large three-dimensional quantities of bubbly mixture were ejected into the outer liquid flow from the main bound cavitation region. Ejection occurring at the trailing edge of the bound cavitation can be deduced in Figure 6c from the spanwise nonuniformity of the trailing edge of the cavity region. The diameters of the bubbles in this mixture were

estimated to be about 1/60 in. (0.04 cm). As the expelled two-phase mixture was carried downstream by the main flow, it continually changed shape and size; occasionally, it appeared to spin with the spin axis parallel to the span. The bubbles collapsed before reaching the trailing edge unless, as occurred at very low values of σ, the main cavity length was large. Occasionally a pocket of very small bubbles appearing as a cloud was swept downstream of the hydrofoil. These bubbles may have been gas filled and their presence has raised speculation that some gaseous diffusion occurred within the main cavity region. The passing of the mixture downstream was often followed by clearly distinguishable, vertically oriented spinning groups of the small bubbles, lower right corner of Figure 6c. These bubbles often persisted downstream of the trailing edge. Their persistence and alignment indicated that they were trapped within the core of a strong vortex. At the spanwise edge of the main cavity region, the recirculation of bubbles in the cavity was apparent.

These observations support the contention that the inception on the nontripped hydrofoil was caused by flow separation as discussed in Section 5. As the cavitation region grew with decreasing σ, the flow pattern of the outer liquid phase was altered causing unsteady turbulent separation at the downstream extremity of the cavity. An ejection process not unlike that occurring in and maintaining turbulent boundary layers existed. In the current case, the ejection of a bubbly volume followed by the sweeping of bubble-filled vortices occurred. We can speculate that this process would also occur in the process of separation of the noncavitating turbulent boundary layers.

The high-speed motion picture of the tripped hydrofoil cavitation showed clearly that separate events occurred which involved growth and splitting of large, single, cavitation bubbles. The film was made immediately after the tunnel was filled with fresh water; thus, σ_i was abnormally low. The condition selected for filming was $\sigma = 0.44$. Still photographs, however, were taken during previous acoustic

measurements using a different tunnel filling, and some of these have been selected to illustrate observed trends of the filmed bubbles. At that time σ_i was higher than it was for the motion picture. Two photographs which show examples of the events are in Figure 11 for $\sigma \approx 0.91$ and in Figure 8 for $\sigma = 0.78$. Relatively near inception, represented by $\sigma = 0.91$ where $\sigma_i = 1.15$ in Figure 11, bubbles began growing spherically, reaching maxima downstream of the point of $C_{p_{min}}$. A few of the bubbles were far enough from the wall so that they grew to a maximum size and then decreased in size, remaining nearly spherical. Nearer to the wall and probably inside the boundary layer where the static pressures were lower, the bubbles grew to a larger size. When downstream of $C_{p_{min}}$ these bubbles took a prolate spheroidal shape with the major axis normal to the plane of the hydrofoil. At their maximum sizes, the tips of the bubbles frequently touched the surface of the hydrofoil. While continuing to travel downstream, the bubbles developed varying degrees of local deformation at the point on the bubble surface closest to the surface of the hydrofoil. A large number of bubbles which were formed even closer to the surface of the hydrofoil took on nearly hemispherical shapes that persisted until after they passed the point of $C_{p_{min}}$. At this point the liquid-phase flow over the bubbles apparently separated as in Figure 8. The part of the bubble adjacent to the hydrofoil became stationary and that part furthest from the surface was carried along with the free stream. This caused stretching of the bubble and the formation of a two-phase mixture. The downstream extremity of this mixture appeared as an unbroken sector of the original bubble while the upstream portion of the mixture appeared to be a collection of small bubbles. As the stretching continued, the downstream extremity began to spin with a spanwise axis of rotation, while the stretched portion appeared as two nearly parallel line filaments of small bubbles which joined the hydrofoil surface with the convected spinning downstream extremity. Thus the flow separation over the bubble caused it to be split; the resulting two-phase vorticity system consisted of a mixture bound to the hydrofoil, a mixture entrained

within two vortex filaments, and a bubbly mixture which was convected in the free stream. The collapse of these individual bubble systems began with the free vortex, followed by the small bubbles in the stretched vortex filaments, then the bubbles in the bound vortex on the hydrofoil. The small bubbles occurring in this cavitation were of the same apparent size as those occurring as a result of the laminar separation.

7. ACOUSTIC CHARACTERISTICS OF THE CAVITATION

CAVITATION ON LOW-PRESSURE SIDE

The spectral densities of radiated sound from the nontripped hydrofoil are shown in Figure 12 for U_∞ = 18 ft/s (5.5 m/s) and α = 4 deg for a range of σ. The spectral density has been referred to a 1-yd (0.9 m) range by using the correction for tunnel reverberation. It is defined as

$$10 \log \overline{p_s^2}\,(f, \Delta f)/\Delta f$$

where $\overline{p_s^2}\,(f, \Delta f)$ is the mean-square pressure at 1 yd (0.9 m), measured in the 1/3-octave bandwidth (Δf) at frequency f. At less than 2 kHz the background levels in the test section dominated the measurement. At more than 6 kHz, the spectral density increased to a maximum near 31.5 kHz.* The spectrum levels for σ = 1.15 are comparable to the background levels. Absorption effects accounted for approximately 1-dB

*An additional peak of f = 3.15 kHz is present in all spectra of noise, yet it cannot be firmly explained by results of the acoustic calibration. It is apparent from calibration that discrete acoustic tunnel modes exist at this low frequency; these modes are expected on theoretical grounds. We speculate that f = 2.5-kHz and f = 3.15-kHz bands are influenced by an interaction of the bubbles with a discrete mode in this region. The test section is not considered reverberant at less than f = 5 kHz. This peak has also been observed in unpublished noise spectra from air-bubble emission.

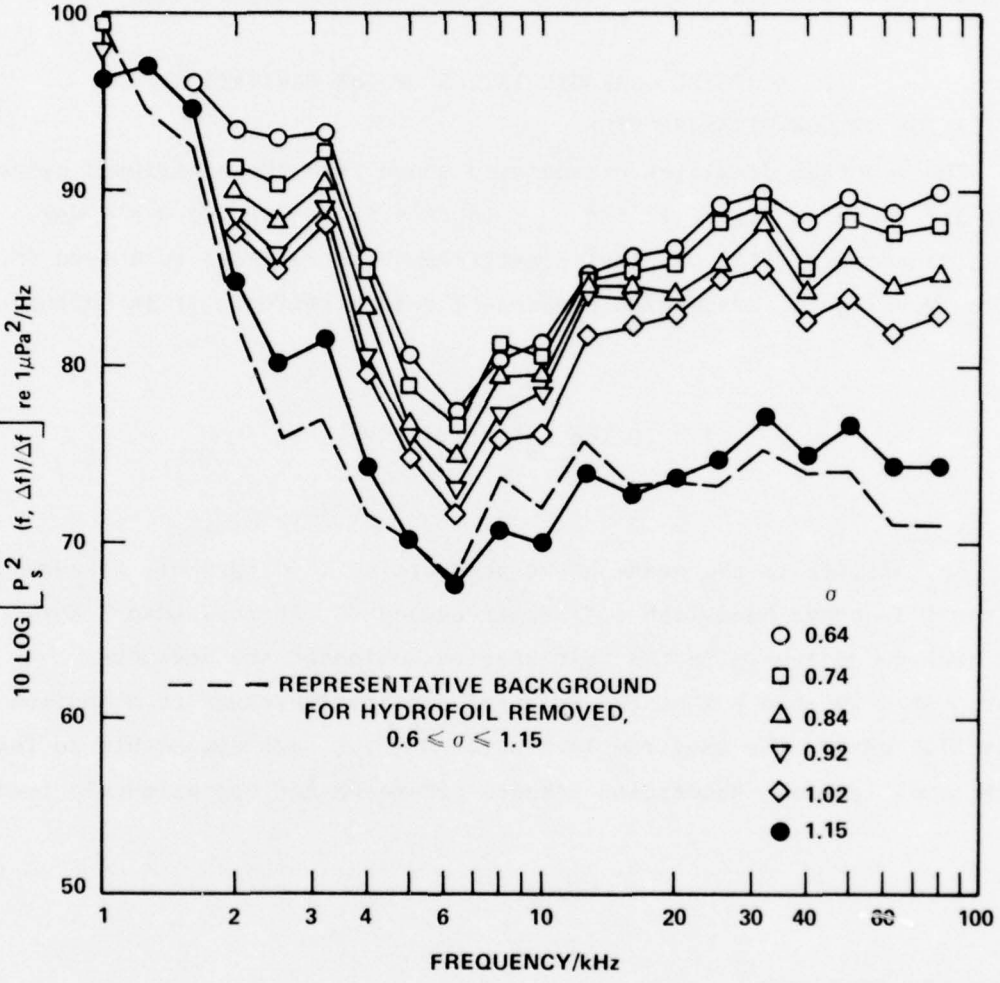

Figure 12 - Spectral Densities, Referred to 1 Yard (0.9 M), of Sound Generated by Separation-Induced Cavitation for U_∞ = 18 Ft/S (5.5 M/S), α = 4 Degrees and 10-Percent Air Content at Atmospheric Pressure

reduction in level near 50 kHz. The noise levels increased abruptly with the onset of cavitation and then continued to increase only slightly with a further reduction in cavitation index. The chordwise length of the major cavity region increased in extent from approximately $0.25 < x/c < 0.38$ at $\sigma = 0.92$ to approximately $0.25 < x/c < 0.7$ at $\sigma = 0.64$. The dependence on σ of the noise levels at 31.5 kHz for four water velocities is shown in Figure 13. An abrupt increase in level for $\sigma < \sigma_i$ occurs for all speeds and it reflects the rapid onset of cavitation. The sound levels in this band for $\sigma \simeq 0.9$ increase roughly as $\overline{p_s^2}(f,\Delta f) \propto U_\infty^4$, as shown by the 6 dB increase in noise in the speed range 16 ft/s (4.9 m/s) to 22 ft/s (6.7 m/s). The levels marked by darkened points correspond to measurements obtained after the tunnel was filled; those marked by open points were obtained after inception conditions had stabilized.

The cavitation noise for the tripped boundary layer is shown in Figure 14. The general shapes of the spectral densities for this case are not unlike those of Figure 12; however, the levels are considerably higher. Near inception the dependence on σ is more gradual for the untripped hydrofoil. Although the tunnel possesses discrete modal properties for $f < 5$ kHz, we have applied the tunnel correction at low frequencies to give estimates of free-field sound. The gradual increase in sound level with reduction in σ is typical of all speeds; see Figure 15. The dependence on σ is much more repeatable for the 31.5-kHz-band levels than for the 3.15-kHz-band levels.

Data for other angles of attack showed that the noise of both cavitation types similarly depended on σ and U_∞. The gradual increase of the traveling bubble cavitation noise with reduction of σ indicated that a uniform increase in the number of available nuclei occurred. Also, as σ decreased, the rate of single events was audibly perceived to increase steadily. For the bound cavitation associated with laminar boundary-layer separation this was not the case. After inception and the abrupt onset of noise, the audible characteristics of the noise were

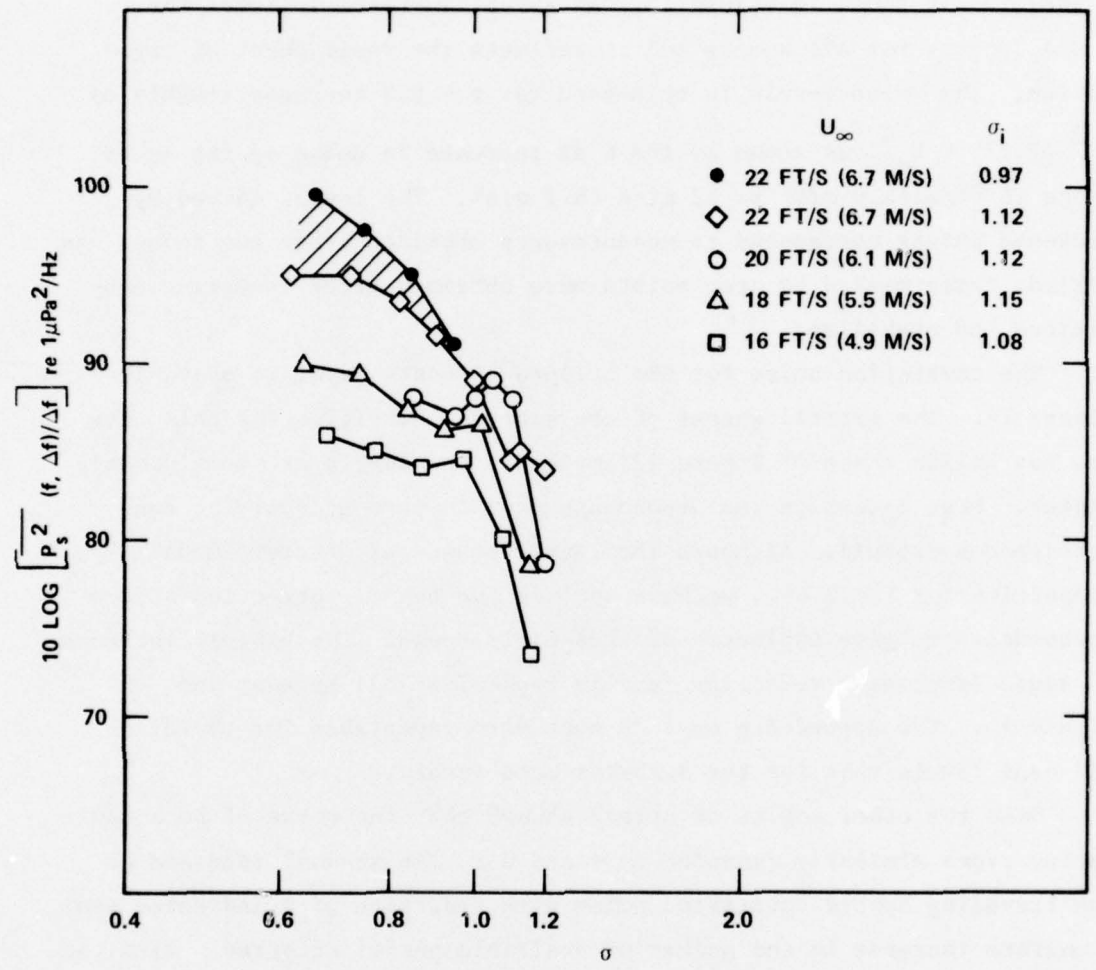

Figure 13 - Sound Spectral Densities at 1 Yard (0.9 M) versus Cavitation Index and Water Speed for the 31.5-kHz-Third-Octave Frequency Band
(Spectra were obtained for no trip and α = 4 degrees)

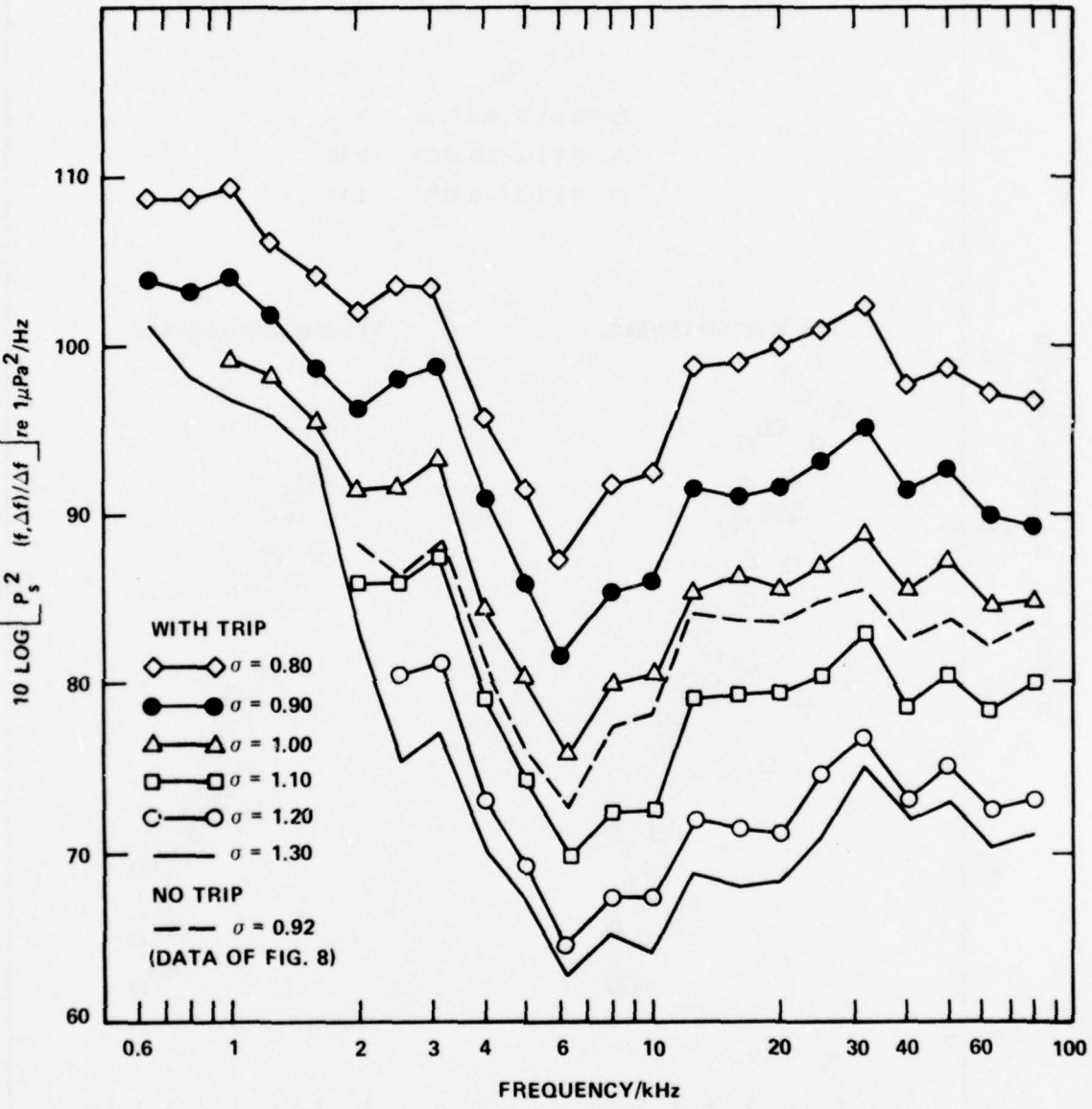

Figure 14 - Spectral Densities at 1 Yard (0.9 M) of Traveling Bubble Cavitation Noise for various Cavitation Indices (Levels are for a tripped boundary layer at U_∞ = 18 ft/s (5.5 m/s), α = 4 degrees, σ_i = 1.15, at 5-percent air content at atmospheric pressure)

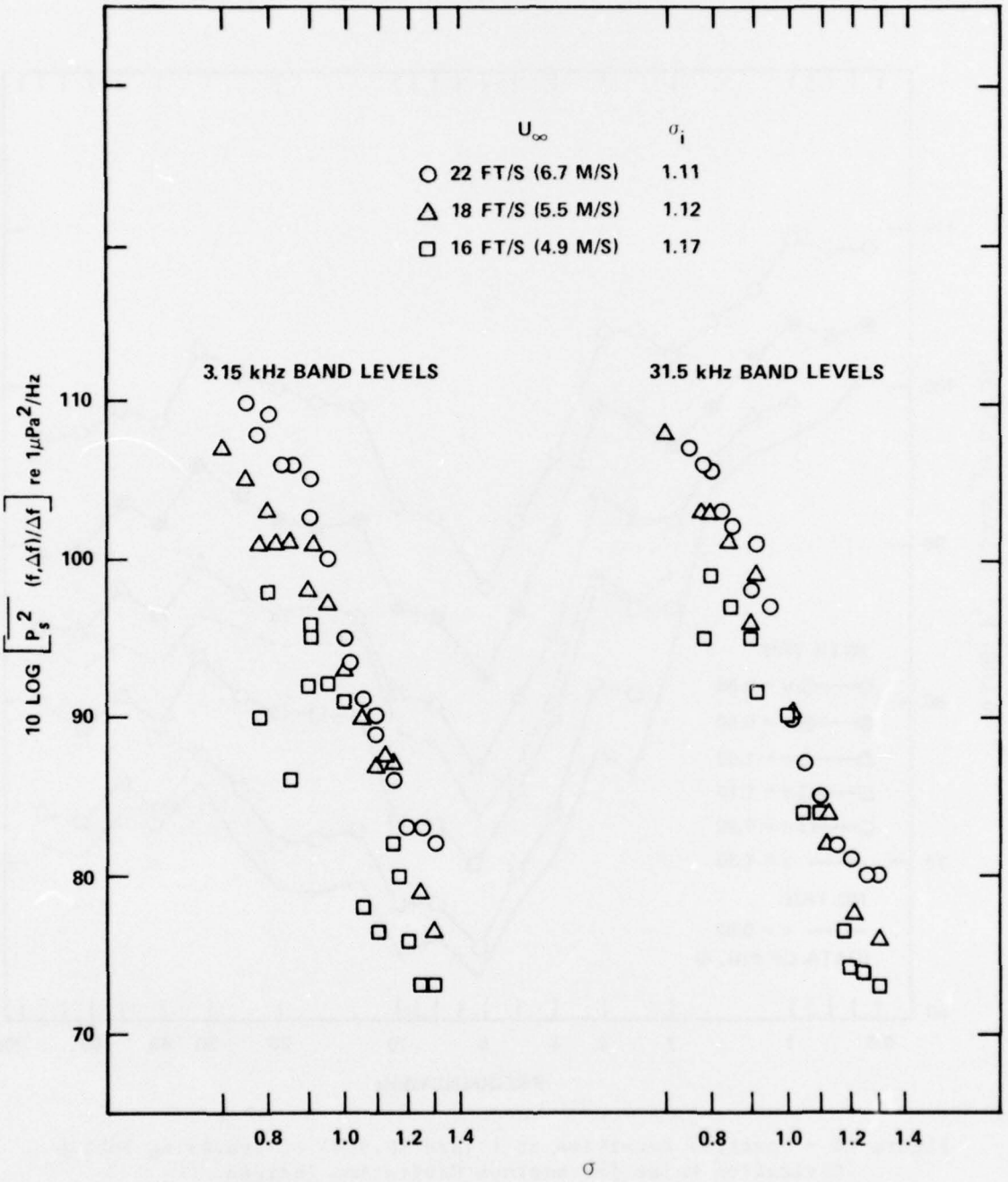

Figure 15 - Dependence on Cavitation Index of Spectral Density Levels at 1 Yard (0.9 M) for Traveling Bubble Cavitation Noise at Various Speeds and α = 4 Degrees

unchanged; yet, the cavity extent increased with a continued reduction in σ. The influence of free-gas content on the noise of both cavitation types was primarily to change σ_i. For the advanced stages of cavitation there was no significant change in noise levels due to slight increases in free gas. It is curious that the high-frequency levels of the spectra are peaked at nearly the same frequency for noise from both types of cavitation. An examination of a large number of enlarged stroboscopic photographs of each type of cavitation disclosed that the diameters of the smallest bubbles in each case were about 1/80 (0.03 cm) to 1/60 in. (0.04 cm). The process of bubble splitting by the liquid flow-separation which was described in the previous section resulted in the small bubbles. The size distribution of these small bubbles probably was controlled by the length scale and the intensity of the turbulence of the liquid flow. This explanation has been given by Sevik and Park (1972)[20] for the splitting of air bubbles by turbulent water jets.

CAVITATION ON HIGH-PRESSURE SIDE

The spectra of noise from cavitation on the high-pressure side of the hydrofoil are shown in Figure 16. For an angle of attack of -2 deg, and U_∞ = 16 ft/s (4.9 m/s), data are shown for $\sigma < 0.98$. To perform this measurement, the hydrofoil was turned so that the high-pressure side faced the hydrophone.* For frequencies less than 8 kHz, the noise at σ = 0.70 was similar to that radiated by the separation-induced cavitation on the low-pressure side. For higher frequencies the mean-square

---

[20] Sevik, M. and S.H. Park, "The Splitting of Drops and Bubbles by Turbulent Fluid Flow," Journal of Basic Engineering, Transactions American Society of Mechanical Engineers, Paper 72WA/FE-32, pp. 1-8 (1972).

* Noise levels from cavitation on the high-pressure side of the hydrofoil were measured on two occasions, with that surface facing toward and facing away from the receiver. The levels differed by more than a factor of 2 for the frequency range from 5 to 20 kHz. This difference is attributed to a shadowing effect of the hydrofoil on the noise.

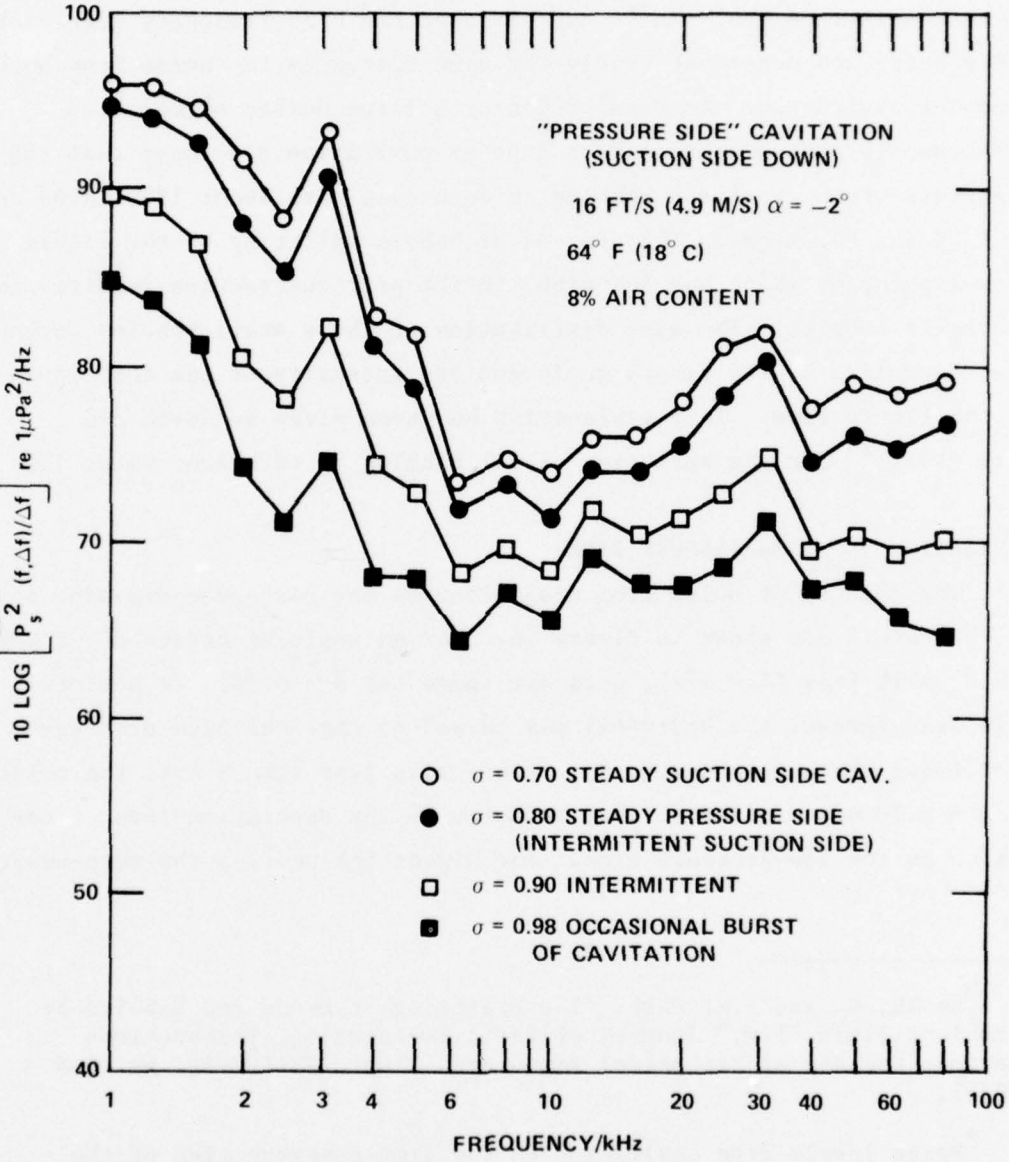

Figure 16 - Spectral Densities of Noise from Cavitation on High-Pressure Side of Hydrofoil for U_∞ = 16 Ft/S (4.9 M/S) and -2 Degrees Angle of Attack

pressures of the noise were approximately a factor of 10 less than those radiated on the low-pressure side either with or without the trip. This cavitation therefore generated less noise at high frequencies than either type on the low-pressure side.

RADIATION FROM CAVITATION-INDUCED VIBRATION

The contribution to the radiated noise from excited structural modes of the hydrofoil were estimated. An accelerometer was mounted on the support shaft of the hydrofoil outside the water tunnel; the shaft was used to vary the angle of attack of the hydrofoil. The accelerometer was sensitive to flexural vibration of the hydrofoil induced by the cavitation. Concurrent measurements of radiated noise and shaft acceleration were obtained for examples of low-pressure-side cavitation with and without a trip.

In a separate set of measurements, the hydrofoil was driven with a shaker mounted at two span locations at midchord--at midspan and at quarter span. This experiment provided a measure of the relationship between the sound levels radiated from structural modes of the hydrofoil and the acceleration measured at the support shaft. The resulting ratios of the sound pressure level at the hydrophone to the shaft acceleration are shown in logarithmic form in Figure 17. The ratios are given for each drive point. The differences in ratios at high frequencies are probably caused by local differences in the flexural impedance of the hydrofoil.

Cavitation-induced sound pressure levels and acceleration levels on the hydrofoil shaft are shown in Figure 18 for no trip and in Figure 19 with a tripped boundary layer. In both cases the cavitation was intermittent. The separate radiation from the structure modes was estimated by multiplying the flow-induced acceleration by the pressure-to-acceleration ratios in Figure 17. The ratio shown by the dotted line in Figure 17 is an upper bound, and it has been used to compute the sound levels in Figures 18 and 19. We see that for frequencies less than 50 kHz, the direct radiation from the cavitation dominates the noise.

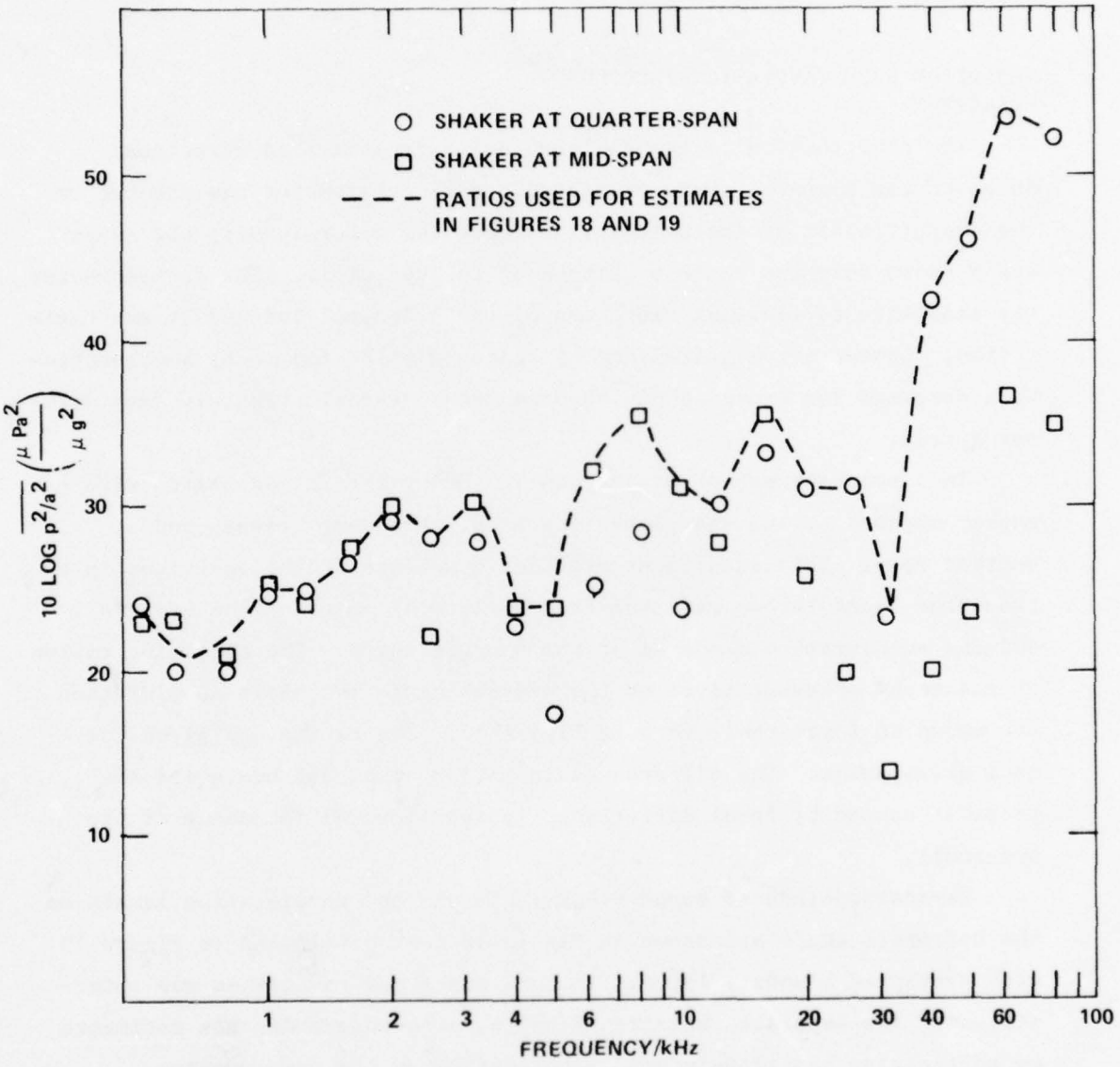

Figure 17 - Ratios of Sound Pressure above Hydrofoil to Acceleration on Hydrofoil Shaft for Two Drive Points

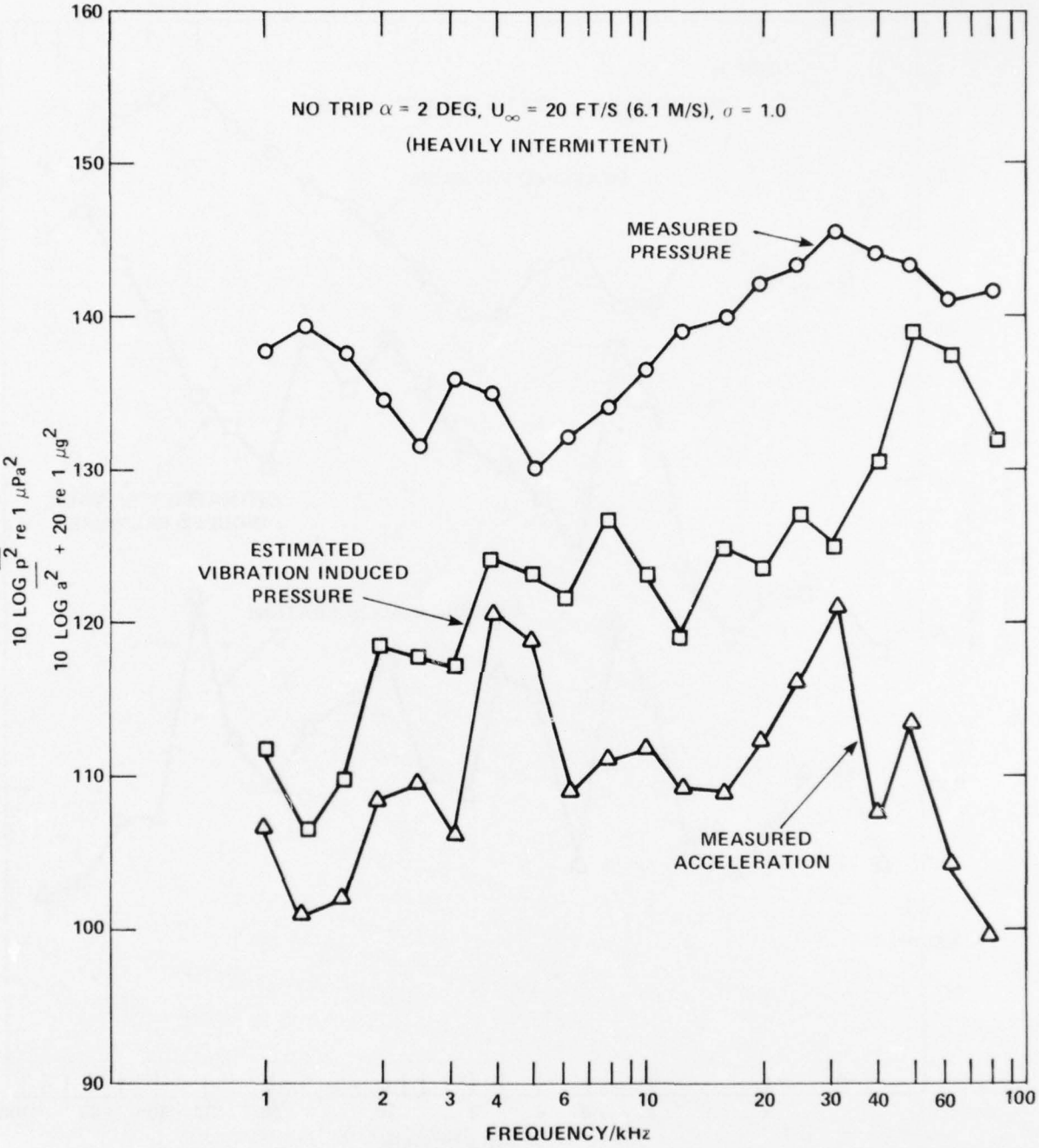

Figure 18 - Sound Pressure and Acceleration Levels Induced by Low-Pressure Side Cavitation without Tripping; Levels are in 1/3-Octave Frequency Bands

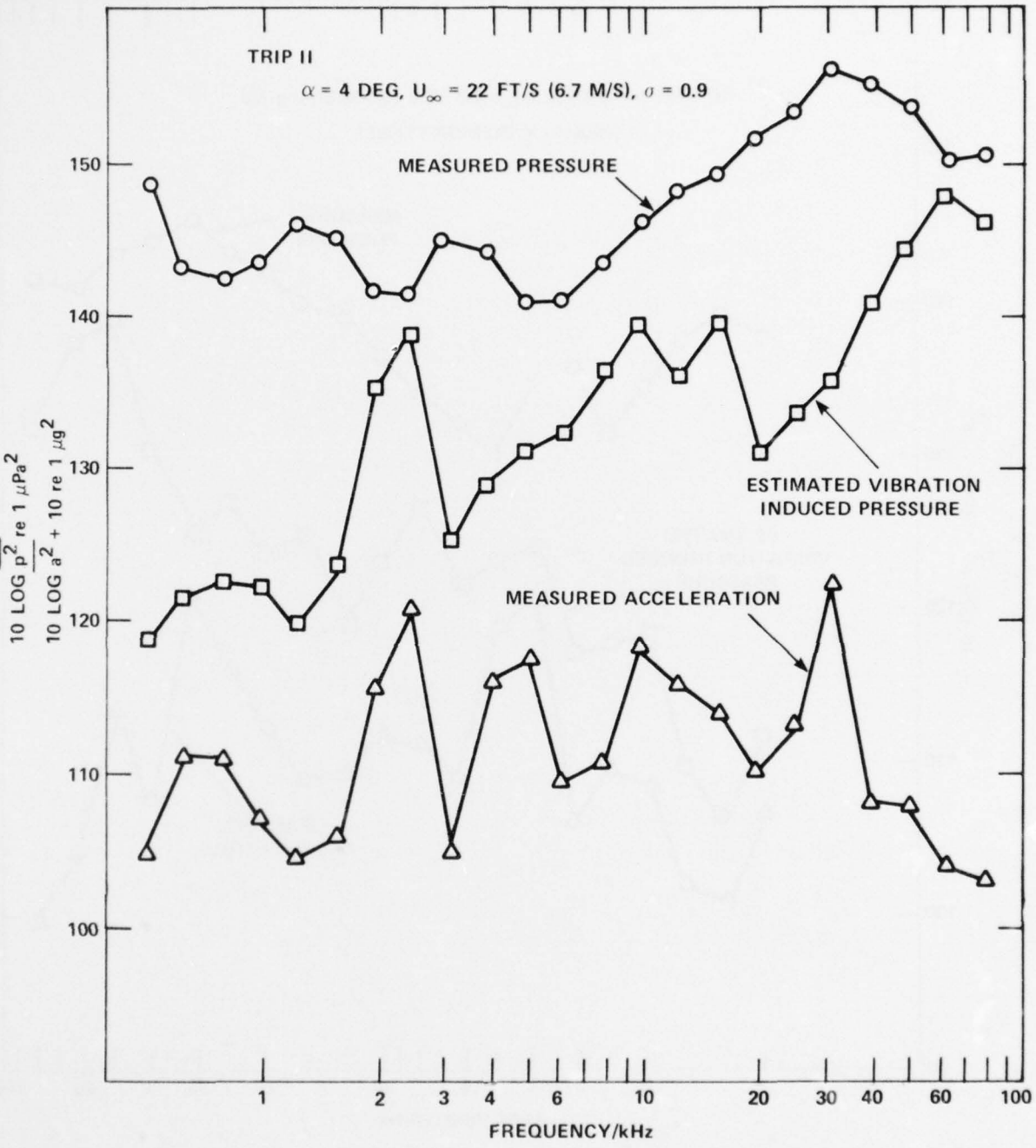

Figure 19 - Sound Pressure and Acceleration Levels Induced by Low-Pressure Side Cavitation with Tripping; Levels are in 1/3-Octave Frequency Bands

The estimated levels at 5 kHz represent upper bounds and they are exceeded by the measured cavitation noise. Thus the frequency spectral content of the noise was established entirely by the cavitation dynamics rather than modal character of the hydrofoil.

8. CONSIDERATIONS OF DYNAMICS OF TRAVELING BUBBLE-CAVITATION NOISE

The high-speed motion pictures of cavitation associated with the tripped boundary layer were used to generate behavior patterns of the bubbles as a function of chordwise location. Figure 20 shows patterns for four of the bubbles that grew on the hydrofoil. The cavitation index was $\sigma = 0.44$, and $U_\infty = 22$ ft/s (6.7 m/s). Twenty events, including both spherical and split bubbles, occurred in the 2-second film, during which the sound level was measured. Included in Figure 20 is the history of a bubble that grew to a hemisphere and then was split by the flow separation around it at $x/c = 0.4$. The other bubbles in Figure 20 were spherical. Superimposed on the bubble diameters are the measured pressure coefficients from Figure 4 as well as the best estimate of the pressure distribution. The continued growth of the bubbles downstream of $C_{p_{min}}$ was similar to that observed by Plesset (1949)[21] on an axisymmetric head form. In the present case one or two rebounds occurred. The maximum spherical bubble radius can be estimated by Strasberg's[19] approximate relationship

$$R_M = \left[\frac{U_\infty^2}{2} \left[-\sigma - C_{p_{min}} \right] \right]^{1/2} t' \qquad (1)$$

where t' is the length of time that it takes for the bubble to pass through the region for which $p < p_v$. In our case

---

[21] Plesset, M.S., "The Dynamics of Cavitation Bubbles," Transactions American Society of Mechanical Engineers, Journal of Applied Mechanics, v. 16, pp. 277-282 (1949).

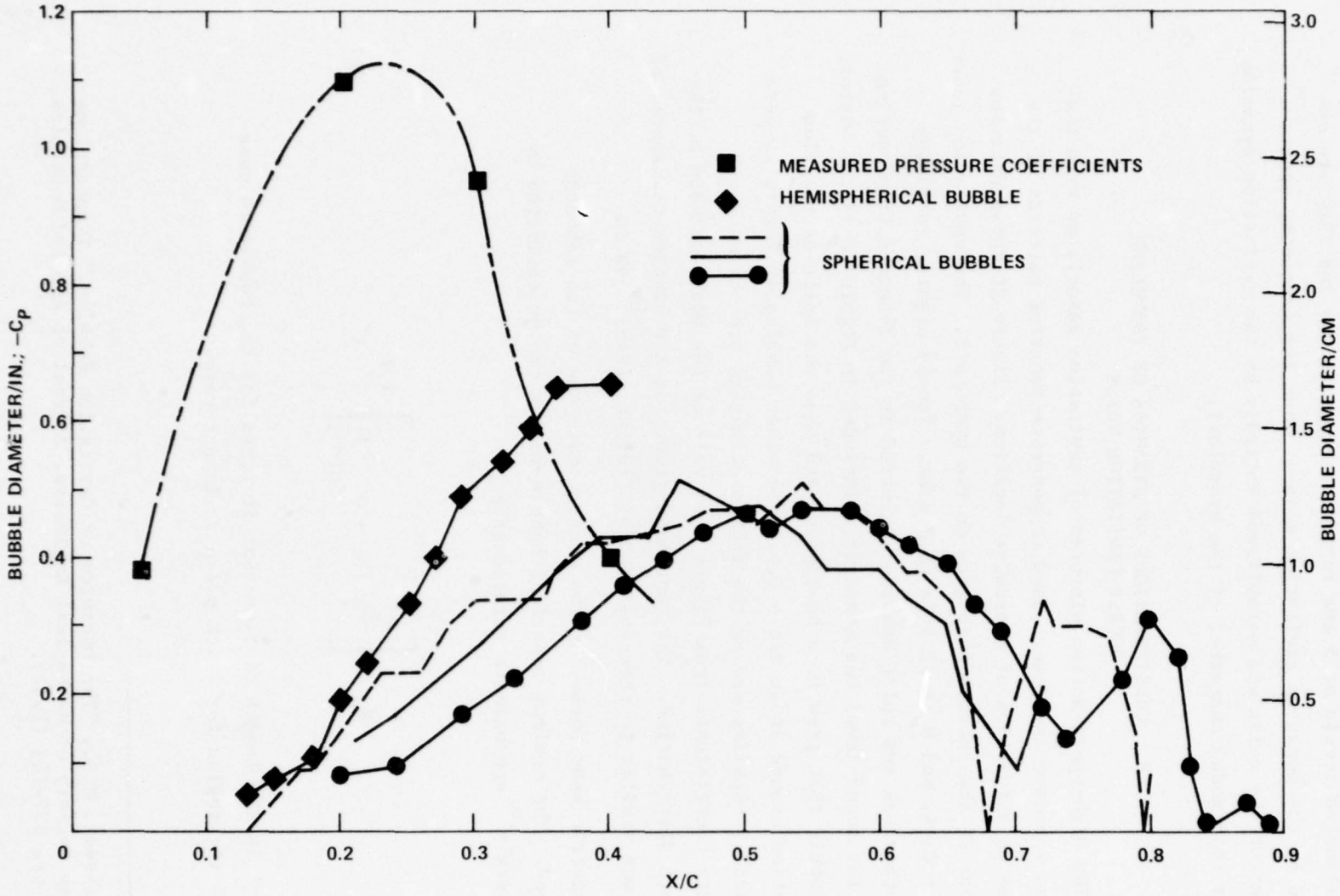

Figure 20 - Filmed Bubble Histories for Traveling Bubble Cavitation, Compared with Measured Pressure Distribution on Tripped Hydrofoil for U_∞ = 22 Ft/S (6.7 M/S), σ = 0.44, α = 4 Degrees

$$t' = \frac{\ell}{U_\infty \left(1-\bar{C}_p\right)} \tag{2}$$

where ℓ is the chordwise extent of this region, and $\bar{C}_p$ is the average static pressure coefficient in the region. Calculations using these equations overestimated the observed maximum bubble radii by approximately 20 percent. Theoretical collapse times (τ_0) for the bubbles, based on the theory of the empty bubble (Lamb (1945)[22]), can be calculated by

$$\begin{aligned} \tau_0 &= 0.915\, R_M \sqrt{\rho/(P_\infty - P_v)} \\ &= 0.915\, \frac{R_M}{U_\infty} \sqrt{2/\sigma} \end{aligned} \tag{3}$$

Calculated values of τ_0 using observed R_M were less than observed collapse times by about 15 percent.

These measurements of the traveling bubble histories are used to estimate the contribution of the dynamics of large bubbles to the traveling bubble cavitation noise in Figure 14. The noise of a single spherical cavitating bubble has been shown by Fitzpatrick and Strasberg (1956)[23] to have a frequency spectral density which is normalized as

$$\frac{S(f)\, r^2}{P_\infty R_M^4 \rho} = S(f\tau_0) \tag{4}$$

Here r is the acoustic range of the noise, and the spectrum is defined as

---

[22] Lamb, H., "Hydrodynamics," Dover Publications (1945).

[23] Fitzpatrick, H. and M. Strasberg, "Hydrodynamic Sources of Sound," First Symposium on Naval Hydrodynamics, Washington, D.C., pp. 241-280 (1956). Also available as DTMB Report 1269 (1959).

$$\int_0^\infty S(f)\, df = \int_0^\infty p_s^2(t)\, dt = \gamma\tau_0\, \overline{p_s^2}$$

where $\gamma\tau_0$ is the total lifetime of the bubble expressed in multiples of τ_0 and where $p_s(t)$ is the sound level from the collapse and $\overline{p_s^2}$ is its time-averaged mean square. For a measurement of sound pressure in a narrow frequency band, this can be rewritten to give

$$S(f) = \frac{\gamma\tau_0 \overline{p_s^2}(f,\Delta f)}{\Delta f} \tag{5}$$

where $\overline{p_s^2}(f,\Delta f)$ is the mean-square pressure in the filter band. From the data of the current study and from calculations of Fitzpatrick and Strasberg,[23] we determine that $\gamma \simeq 3$. The spectral density of the sound generated by the bubbles of Figure 20 is shown in Figure 21. Note that these levels at high frequency are comparable to those in Figure 11 for $\sigma = 0.8$ and 0.9; however, the peak levels, excepting the peak at $f = 3.15$ kHz, occur at a lower frequency than in Figure 14. Normalization of data from Figure 14 as well as from Figure 21 gives spectra in Figure 22 in the dimensionless form

$$S(\tau_0 f) = \frac{\overline{p_s^2}(f,\Delta f)}{\Delta f} \frac{\gamma\tau_0\, r}{R_M^4\, \rho P_\infty} . \tag{6}$$

Note that the frequency of the peak in the high-frequency spectrum for $\sigma = 0.44$, and $U_\infty = 22$ ft/s (6.7 m/s), now more nearly corresponds with that frequency for $\sigma = 0.9$, and $U_\infty = 18$ ft/s (5.5 m/s), than it did when it was not normalized. We compare the measured normalized spectra to the theoretical spectrum for single bubble-cavitation noise computed by Fitzpatrick and Strasberg[23] in the same figure. In making this

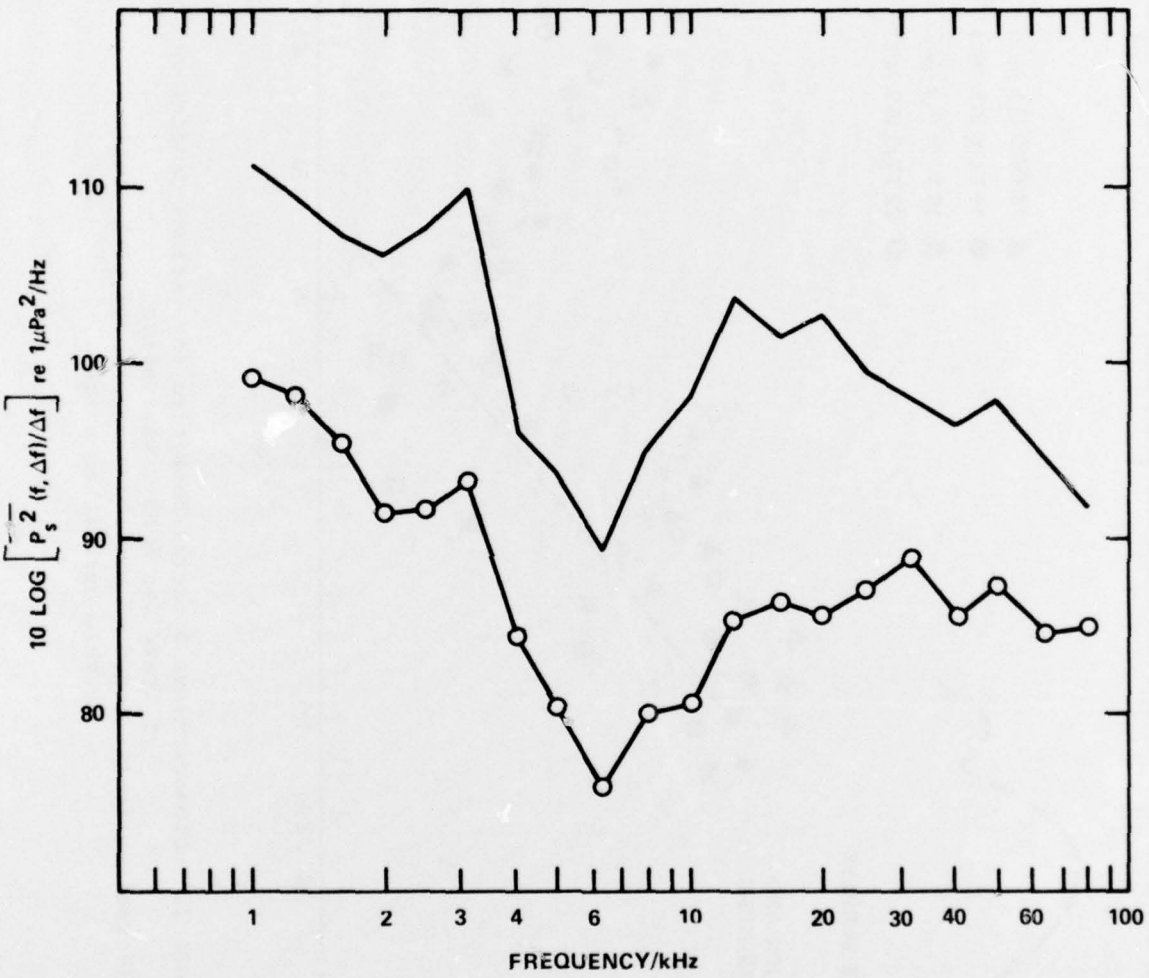

Figure 21 - Spectral Densities at 1 Yard (0.9 M) for Traveling Bubble Cavitation (Noise spectrum obtained during filming of bubbles in Figure 13, σ = 0.44, U_∞ = 22 ft/s (6.7 m/s) (——); spectrum from Figure 11, σ = 0.9, U_∞ = 18 ft/s (5.5 m/s) (-o-o-)

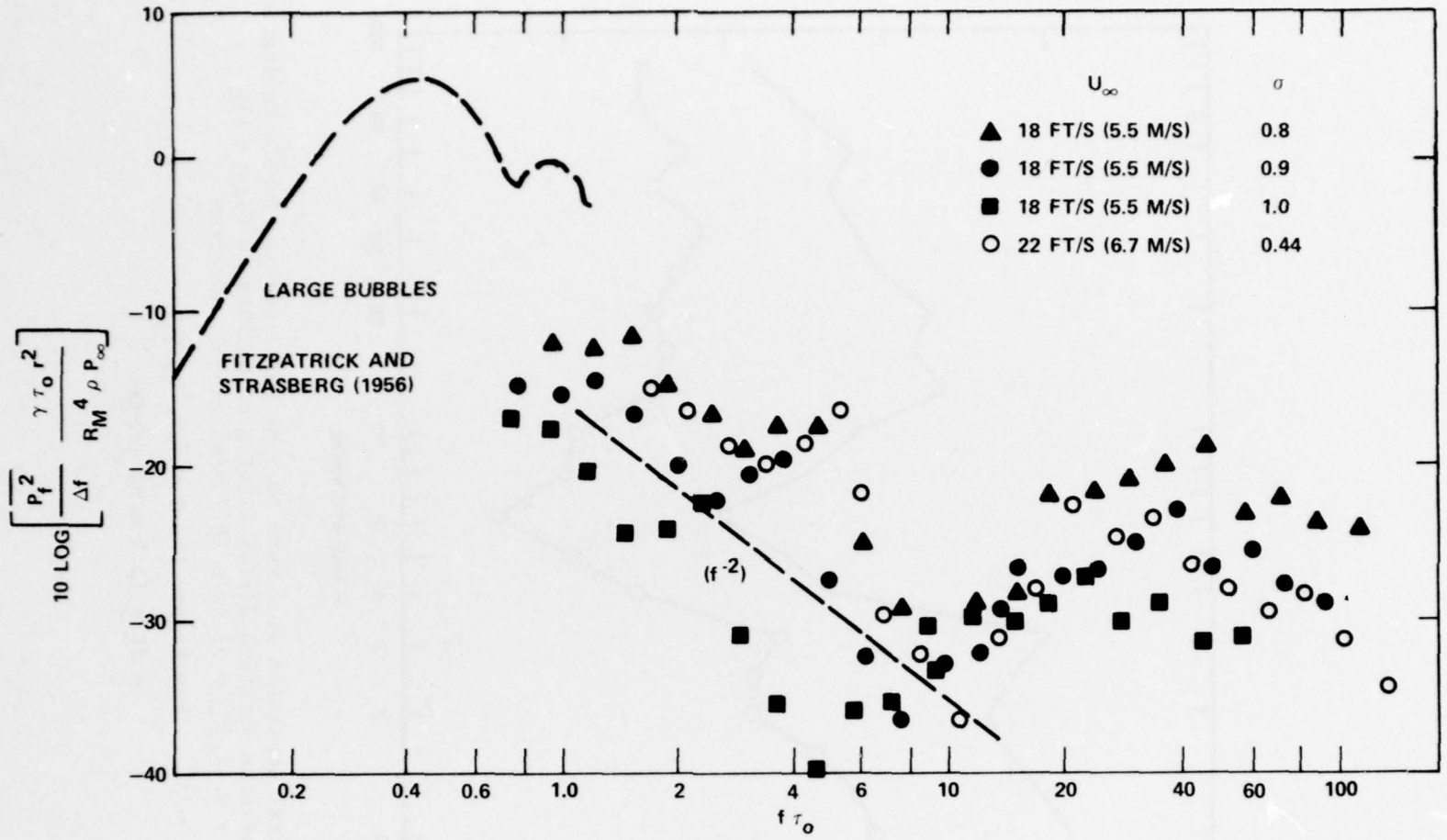

Figure 22 - Dimensionless Spectral Densities for various Conditions of Traveling Bubble Cavitation
(Normalization is based on variables associated with single-bubble cavitation noise)

comparison we have assumed statistically independent events which occur at the rate of one each second. Actually, during the motion picture, the rate of large spherical bubble events was greater. For the other conditions the rate was unknown. The comparison serves to show that if the water tunnel background had been low enough, and if the unaccounted 3.15-kHz acoustic reverberation effect had not existed in the tunnel, the noise corresponding to the large-scale bubble motions would have been measured. It appears that the measured spectra were dominated by the final stages of collapse of the large bubbles and by the splitting and reformation of the small ones. The spread in the normalized data of Figure 22 demonstrates the uncertainty in the event rate of bubble collapses. We interpret the higher dimensionless levels at $\sigma = 0.8$ for $U_\infty = 18$ ft/s (5.5 m/s), compared to those at $\sigma = 1.0$ at the same speed, as being due to a higher rate of bubble events at the lower cavitation index. As discussed in Section 5, it is reasonable to expect that as σ dropped below σ_i, a larger number of nuclei should have become available as cavitation sites. Some further aspects of the scaling and modeling of event rates have been examined by Baiter (1974),[24] who points out many uncertainties in the establishment of event rates. Aside from the unknown distributions of nuclei, Il'ichev and Lesunovskii (1963)[25] show that the probability distribution of events can depend on the statistical nature of turbulence in the flow. The high-speed photography indicated the existence of a ratio of large-to-small bubble sizes of approximately 50. A translation of the theoretical noise peak from $f\tau_0 = 0.5$ to $f\tau_0 = 25$ to account for the characteristic collapse time, which is proportional to bubble radius, of the smaller bubbles causes the theoretical peak to correspond roughly with that in

---

[24] Baiter, H.J., "Aspects of Cavitation Noise," Symposium on High Powered Propulsion of Large Ships, Wageningen, The Netherlands (1974).

[25] Il'ichev, V.I. and V.P. Lesunovskii, "On the Noise Spectra Associated with Hydrodynamic Cavitation," Soviet Physics - Acoustics, v. 9, pp. 25-28 (1963).

the dimensionless spectrum of Figure 22. In the range of $1 < f\ \tau_0 < 10$ the dependence $(f\tau_0)^{-2}$ roughly fits the trend of the data. Unfortunately the peak at f = 3.15 kHz distorts this frequency dependence. A similar dependence has been observed by Jorgensen (1961)[26] for noise from cavitating jets and by Mellen (1954)[27] for noise produced by cavitation from a rotating rod. This frequency dependence has been discussed by Fitzpatrick and Strasberg[23] and more recently by Baiter[24] as being associated with the influence of compressibility of the water. In this connection, we note that the dimensionless form of Equation (6) may be recast in terms of flow variables, using the preceding equations. This results in a U_∞^3-speed dependence for the mean-square radiated pressure at scaled frequencies so that $S(\tau_0 f)$ is constant. An assumption that at fixed σ, the event rate is proportional to U_∞ = 18 ft/s (5.5 m/s), α = 4 deg and σ = 0.74 is in the range

$$\frac{|p_s|r}{R_M P_\infty} \simeq 4 \quad .$$

It is curious that this value is only one-tenth that observed by Harrison (1952)[28] for single cavitation bubbles, which were formed either in a venturi tube or by a spark.

9. SUMMARY

The noise from bound cavitation has been demonstrated, for the hydrofoil examined, to be dependent on viscous effects as brought about by changes in the boundary layer. When laminar boundary-layer separation occurred, considerable noise was produced at high frequencies, probably

---

[26] Jorgensen, D.W. "Noise from Cavitating Submerged Water Jets," Journal of the Acoustical Society of America, v. 33, pp. 1334-1338 (1961).

[27] Mellen, R.H., "Ultrasonic Spectrum of Cavitation Noise in Water," Journal of the Acoustical Society of America, v. 26, pp. 356-360 (1954).

[28] Harrison, M., "An Experimental Study of Single Bubble Cavitation Noise," DTMB Report 815 (1952).

by the formation of small bubbles. These bubbles were carried in groups within vortex filaments of long length which were ejected into the non-cavitating free stream from the bound cavity. At a given speed, the bound cavity increased in size as the cavitation coefficient decreased; however, after inception of cavitation, radiated sound levels increased slowly with further decreasing cavitation index. An increase in extent of cavitation apparently did not cause a proportional increase in the number of uncorrelated bubble events. On the high-pressure side, cavitation consisted of sheets of cavities, and the noise emitted was less intense than that emitted by cavitation on the low-pressure side. In all cases the hydrofoil vibration induced by the cavitation did not contribute to the emitted noise.

When laminar separation was eliminated by tripping the boundary layer into turbulence, inception was delayed and traveling bubble cavitation occurred. For this type, the magnitude of noise was generally greater than that produced by the bound cavitation due to separation. The noise mechanism was complicated by local flow separation around those bubbles closest to the surface of the hydrofoil. This caused the disintegration of large hemispherical bubbles into restricted collections of small ones, causing high-frequency noise. Large bubbles which were suitably far from the hydrofoil surface maintained a nearly spherical shape during growth and collapse, and these produced low-frequency noise which was estimated. The dependence of the measured noise on the cavitation index after inception was much greater in comparison with the cavitation associated with laminar separation. For the traveling bubble cavitation, a continued reduction in cavitation index brought on a larger number of nearly independent bubble events, and these caused increasing levels of noise. A marked difference between the two cavitation types in the dependence of noise on cavitation index was thus observed.

In comparing the noise radiated by the two types of cavitation on the low-pressure side we note that since inception was slightly delayed by tripping, the onset of noise was also delayed. However, even though

inception was delayed, the noise actually exceeded the separation-induced cavitation noise by several decibels in the more advanced stages of traveling bubble cavitation. We speculate that this is the combined effect of more statistically independent events in the latter case as well as more gaseous diffusion brought about by long residence times in the cavity zone in the untripped case. Both the noise and inception results have raised speculation that changes in nucleus content could affect different cavitation types in different ways, viz, traveling bubble, compared to bound cavitation.

A simple scaling of the traveling bubble-noise spectrum was probably limited by an unknown characterization-of-event rates by flow variables as well as the uncertainty in physical quantities which affect the dynamics of the small-size bubbles. Although it has been speculated that these bubbles were generated by splitting large ones by turbulent separation, we have not yet quantified the flow variables which control the process.

ACKNOWLEDGMENTS

The authors appreciate helpful discussions with Drs. M. Sevik and M. Strasberg concerning aspects of bubble and cavitation dynamics and with Dr. F. Peterson concerning viscous effects on cavitation inception. The work was sponsored by the David W. Taylor Naval Ship Research and Development Center In-House Independent Research Program.

REFERENCES

1. Liebeck, R.H., "A Class of Airfoils Designed for High Lift in Incompressible Flow," Journal of Aircraft, v. 10, No. 10, pp. 610-617 (Oct 1973).

2. Glauert, H., "The Lift and Drag of a Wing Spanning A Free Jet," Aeroanutical Research Council (Great Britain) R&M 1603 (Mar 1934).

3. Diprose, K.V., "Drag Tests on a Fabric-Covered and a Polished-Plywood Wing in the 24-Ft Tunnel," Aeronautical Research Council (Great Britain) R&M 1813 (Mar 1937).

4. Tulinius, J.R., "Theoretical Prediction of Wing-Fuselage Aerodynamic Characteristics at Subsonic Speeds," North American Rockwell Corporation Report NA-69-789 (1969).

5. Tulinius, J.R., "Theoretical Prediction of Thick Wing Aerodynamic Characteristics at Subsonic Speeds," North American Rockwell Corporation Report NA-70-104 (Oct 1970).

6. Wang, H.T., "Comprehensive Evaluation of Six Thin-Wing, Lifting-Surface Computer Programs," NSRDC Report 4333 (Jun 1974).

7. Hall, D.J. and J.C. Gibbings, "The Influence of Stream Turbulence and Pressure Gradient upon Boundary Layer Transition," Journal of Mechanical Engineering Sciences, v. 14, pp. 134-146 (1972).

8. Schlichting, H., "Boundary Layer Theory," McGraw-Hill, Inc. (1960).

9. Holl, J.W. et al., "Limited Cavitation and the Related Scale Effects Problem," Second International Japanese Society of Mechanical Engineers Symposium (1972).

10. Peterson, F.B., "Water Tunnel--High-Speed Basin Cavitation Inception Comparison," 12th International Towing Tank Conference, pp. 519-523 (1969).

11. Arakeri, V.H. and A.J. Acosta, "Viscous Effects in the Inception of Cavitation on Axisymmetric Bodies," Journal of Fluids Engineering, American Society of Mechanical Engineers, v. 95, Ser. 1, No. 4, pp. 519-528 (1973).

12. Acosta, A.J., "Cavitation and Fluid Machinery," Cavitation Conference, Edinburg, Scotland (1974).

13. Casey, M.V., "The Inception of Attached Cavitation from Laminar Separation Bubbles on Hydrofoils," Cavitation Conference, Edinburg, Scotland (1974).

14. Arakeri, V.H., "A Note on the Transition Observations on an Axisymmetric Body and Some Related Fluctuating-Wall Pressure Measurements," Journal of Fluids Engineering, Transactions American Society of Mechanical Engineers, v. 97, Ser. 1, No. 1, pp. 82-86 (1975).

15. Blake, W.K., "Statistical Description of Pressure and Velocity Fields at Trailing Edges," NSRDC Report 4241 (1975).

16. Arndt, R.E.A. and A.I. Ippen, "Cavitation Near Surfaces of Distributed Roughness," Massachusetts Institute of Technology Hydrodynamics Laboratory Report 104 (1967).

17. Brockett, T. "Some Environmental Effects on Headform Cavitation Inception," NSRDC Report 3974 (1972).

18. Peterson, F.B., "Hydrodynamic Cavitation and Some Considerations of the Influence of Free-Gas Content," Ninth Symposium on Naval Hydromechanics, Paris, France (1972).

19. Strasberg, M., "The Influence of Air-Filled Nuclei on Cavitation Inception," DTMB Report 1078 (1956).

20. Sevik, M. and S.H. Park, "The Splitting of Drops and Bubbles by Turbulent Fluid Flow," Journal of Basic Engineering, Transactions American Society of Mechanical Engineers, Paper 72WA/FE-32, pp. 1-8 (1972).

21. Plesset, M.S., "The Dynamics of Cavitation Bubbles," Transactions American Society of Mechanical Engineers Journal of Applied Mechanics, v. 16, pp. 277-282 (1949).

22. Lamb, H., "Hydrodynamics," Dover Publications (1945).

23. Fitzpatrick, H. and M. Strasberg, "Hydrodynamic Sources of Sound," First Symposium on Naval Hydrodynamics, Washington, D.C., pp. 241-280 (1956). Also available as DTMB Report 1269 (1959).

24. Baiter, H.J., "Aspects of Cavitation Noise," Symposium on High Powered Propulsion of Large Ships, Wageningen, The Netherlands (1974).

25. Il'ichev, V.I. and V.P. Lesunovskii, "On the Noise Spectra Associated with Hydrodynamic Cavitation," Soviet Physics - Acoustics, v. 9, pp. 25-28 (1963).

26. Jorgensen, D.W., "Noise from Cavitating Submerged Water Jets," Journal of the Acoustical Society of America, v. 33, pp. 1334-1338 (1961).

27. Mellen, R.H., "Ultrasonic Spectrum of Cavitation Noise in Water," Journal of the Acoustical Society of America, v. 26, pp. 356-360 (1954).

28. Harrison, M. "An Experimental Study of Single Bubble Cavitation Noise," DTMB Report 815 (1952).

INITIAL DISTRIBUTION

Copies		Copies	
2	ONR	1	American Univ
	1 H.M. Fitzpatrick 468		Prof Mark Harrison
	1 Dr. Perrone 439		Dept of Physics
3	NRL	5	California Inst of of Tech
	1 Dr. Hansen		1 Dr. A.J. Acosta
	1 O.M. Griffin		1 Dr. F.R. Hama
	1 R.A. Skop		1 Dr. A. Roshko
			1 Dr. T.Y. Wu
3	USNA		1 Dr. M.S. Plesset
	1 Dr. Bruce Johnson		
	1 Dr. S. Elder	1	Univ of California,
	1 Library		Los Angeles
			1 Prof W.C. Meecham
1	NAVPGSCOL, Monterey, CA		Dept of Engr
	Dr. Turgut Sarpkaya		1 Prof J.V. Wehausen
			College of Engr
1	USNROTC & NAVADMINUMIT		1 Library
1	NAVWARCOL	2	Univ of Calif, San Diego
			1 Prof J.W. Miles
3	NUC, San Diego, CA		Inst of Geophysics &
	1 Dr. A. Fabula		Planetary Physics
	1 Dr. J. Hoyt		1 T.T. Yeh
	1 Mr. H. Patrick		
		2	Univ of Southern California
3	NLONLAB, NUSC		Los Angeles
	1 Dr. H. Bakewell		1 Dr. J. Laufer
	1 Dr. H. Schloemer		Dept Aero Space Engr
	1 Dr. W. Strawderman		1 Dr. R. Blackwelder
1	NEWPORT, NUSC	3	Catholic Univ of America
	1 R.N. Brown		1 Dr. F.A. Andrews
			1 Dr. M. Casarella
2	NAVSEA		1 Dr. R. Smith
	1 SEA 037		
	1 SEA 0372 (A. Paladino)	1	Colorado State Univ
			Prof M. Albertson
2	NAVSEC		Dept of Civ Engr
	1 SEC 6110		
	1 SEC 6148	1	Univ of Connecticut
			Prof V. Scottron
1	National Bureau of Standards		Hydr Res Lab
	Mr. P.S. Klebanoff		
12	DDC		

Copies	
2	Georgia Inst of Tech 1 Dr. A.D. Pierce 1 Dr. A.W. Morris
2	Harvard Univ 1 Dr. R.E. Kronauer Div of Eng & Appl Physics 1 Prof G. Birkhoff Dept of Math
1	Univ of Hawaii M. St. Denis Dept of Ocean Engr
1	Univ of Houston Dr. A.K.M.F. Hussain Dept of Mech Engr
1	Illinois Inst of Tech M.V. Morkovin Dept of Mech & Aero
1	Univ of Illinois J.M. Robertson Theor & Applied Math
3	Univ of Iowa 1 Hunter Rouse 1 L. Landweber Inst of Hydro Res 1 J. Kennedy
7	MIT 1 Dr. R.H. Lyon Dept Mech E 1 Dr. S. Crandall Dept Mech E 1 Dr. P. Leehey Dept NAME 1 Dr. Ira Dyer Dept NAME 1 Prof P.M. Morse Dept Physics 1 Prof K.U. Ingard Dept Physics 1 Prof. J.E. Kerwin Dept NAME

Copies	
5	Univ of Michigan 1 Prof W.W. Willmarth Dept of Aero & Astro Engr 1 Prof T.F. Ogilvie 1 Prof R.B. Couch 1 Prof H. Nowaki
3	Univ of Minnesota 1 Prof R. Plunkett 1 Prof B. Lambert 1 Mr. J.M. Killen St. Anthony Falls Hydraulic Lab
1	Montana State Univ Dept of Aero & Mech Engr
2	Univ of Notre Dame Engr Sciences Dept 1 Dr. A.F. Strandhagen 1 Prof A.A. Szewcyzk
2	Ohio State Univ 1 Dr. Robert S. Brodkey 1 Dr. Harry C. Hershey
1	Oregon State Univ School of Engr Prof Larry S. Slotta
5	ARL, Penn State Univ 1 Dr. B. Parkin 1 Dr. E.J. Skudrzyk 1 Dr. R. Arndt 1 Dr. R. Henderson 1 Dr. D. Thompson
2	Stanford Univ 1 Dr. S. Kline 1 Dr. H. Ashley
2	SWRI 1 Dr. Wilfred Baker 1 Editor, Applied Res Review

Copies	
2	SIT/DL 1 Dr. J. Breslin 1 Dr. R.J. Morgan
1	Argonne National Lab H. Chung
1	Binary Systems Inc., N.Y. Mr. S. Gardner
1	BHRA Fluid Engineering Dr. Roger King
1	Bolt Beranek & Newman, Inc. Arlington, VA Dr. F. Jackson
8	Bolt Beranek & Newman, Inc. Cambridge, MA 1 Dr. N.A. Brown 1 Dr. D. Chase 1 Dr. P. Smith 1 Dr. K.L. Chandiramani 1 Dr. J. Barger 1 Mr. R. Hayden 1 Dr. P. Jameson 1 Dr. C.E. Hanson
1	Calspan, Inc. Applied Math Dept
1	Cambridge Acoustical Assoc. Dr. M.C. Junger
3	Combustion Engineering Inc. M. Wolpert
1	Gen Applied Sci Lab Inc. Westbury, N.Y. Dr. F. Lane
4	Electric Boat Div, Gen Dyn. 1 Mr. William Ezell 1 Mr. Michael Pakstys, Jr. 1 Dr. T. Graham 1 Mr. R. Gorman

Copies	
1	Silencing Technology Assoc. Box 695, Bayview, Idaho 83803 Gerald J. Franz
4	Hydronautics, Inc. 1 P. Eisenberg 1 M. Tulin 1 J. Dunne 1 J.O. Scherer
1	Hydrospace Res Corp Library
1	McDonnell Douglas Corp. Dr. R.H. Liebeck
1	Tetratech Inc. Dr. D. Ross
1	Dr. A.A. Hudimac

CENTER DISTRIBUTION

Copies	Code	
1	15	W. Cummins
1	1502	V. Monacella
1	1505	S. Crump
1	1506	M. Ochi
1	152	R. Wermter
1	154	W. Morgan
1	1544	R. Cumming
1	1544	R. Miller
1	1544	T. Brockett
1	1544	S. Jessup
1	1544	D. Valentine
1	1552	J. McCarthy
1	1552	T. Huang
1	1552	F. Peterson
10	1552	H. Wang
1	1552	J. Power
1	1556	G. Santore
1	1556	E. Rood
1	19	M. Sevik
1	1901	M. Strasberg
1	1902	G. Maidanik
1	1903	G. Chertock
1	1905	R. Biancardi
1	1926	D. Vendittis
1	1926	S. Solomon
1	1926	R. Tompkins

Copies	Code	
1	1932	J. O'Donnell
1	1933	J. Lee
1	1936	C. Devin
1	194	
1	194	F. Schloss
1	1942	J. Shen
10	1942	W. Blake
1	1942	B. Bowers
1	1942	R. Brown
1	1942	F. DeMetz
1	1942	G. Finkelstein
10	1942	F. Geib
1	1942	P. Granum
1	1942	L. Maga
1	1942	T. Mathews
1	1942	D. Paladino
1	1942	A. Tucker
1	1942	G. Wilson
1	196	D. Feit
1	1962	A. Zaloumis
1	1965	M. Rumerman
1	1965	F. Desiderati
1	1966	S. Lee
1	1966	Y. Liu
1	197	W. Reader
30	5214.1	Reports Distribution
1	522.1	Unclassified Library (C)
1	522.2	Unclassified Library (A)